Structural Chemistry (2022) 33:1645–1665
https://doi.org/10.1007/s11224-022-01996-y

ORIGINAL RESEARCH

In silico discovery of multi-targeting inhibitors for the COVID-19 treatment by molecular docking, molecular dynamics simulation studies, and ADMET predictions

Aso Hameed Hasan[1,2] · Narmin Hamaamin Hussen[3] · Sonam Shakya[4] · Joazaizulfazli Jamalis[2] · Mohammad Rizki Fadhil Pratama[5,6] · Subhash Chander[7] · Harsha Kharkwal[7] · Sankaranarayanan Murugesan[8]

Received: 31 March 2022 / Accepted: 13 June 2022 / Published online: 6 July 2022

Abstract

Coronavirus disease-2019 (COVID-19), a global pandemic, has currently infected more than 247 million people around the world. Nowadays, several receptors of COVID-19 have been reported, and few of them are explored for drug discovery. New mutant strains of COVID-19 are emerging since the first outbreak of disease and causing significant morbidity and mortality across the world. Although, few drugs were approved for emergency uses, however, promising drug with well-proven clinical efficacy is yet to be discovered. Hence, researchers are continuously attempting to search for potential drug candidates targeting the well-established enzymatic targets of the virus. The present study aims to discover the antiviral compounds as potential inhibitors against the five targets in various stages of the SARS-CoV-2 life cycle, i.e., virus attachments (ACE2 and TMPRSS2), viral replication, and transcription (M^{pro}, PL^{pro} and RdRp), using the most reliable molecular docking and molecular dynamics method. The ADMET study was then carried out to determine the pharmacokinetics and toxicity of several compounds with the best docking results. To provide a more effective mechanism for demonstrating protein–ligand interactions, molecular docking data were subjected to a molecular dynamic (MD) simulation at 300 K for 100 ns. In terms of structural stability, structure compactness, solvent accessible surface area, residue flexibility, and hydrogen bond interactions, the dynamic features of complexes have been compared.

Keywords COVID-19 · Antiviral compounds · Molecular docking · Molecular dynamics · ADMET

Introduction

Since 2 years, the first case of SARS-CoV-2 was reported in Wuhan, China; various variations of concern (VOC) have emerged around the world, with some variants appearing to pose a higher risk to public health, resulting in increased transmissibility or cause more severe disease [1–3]. According to the latest reports from the World Health Organization (WHO), the total number of COVID-19 cases worldwide exceeded 500 million as of April 24, 2022, resulting in more than six million deaths [4]. Several spikes have been observed throughout the world since the outbreak of the

✉ Aso Hameed Hasan
aso.hameed@garmian.edu.krd

1 Department of Chemistry, College of Science, University of Garmian, Kalar, Kurdistan Region-Iraq 46021, Iraq

2 Department of Chemistry, Faculty of Science, Universiti Teknologi Malaysia, 81310 Johor Bahru, Johor, Malaysia

3 Department of Pharmacognosy and Pharmaceutical Chemistry, College of Pharmacy, University of Sulaimani, Sulaimani 46001, Iraq

4 Department of Chemistry, Faculty of Science, Aligarh Muslim University, Aligarh 202002, India

5 Doctoral Program of Pharmaceutical Sciences, Universitas Airlangga, Soekarno Kampus C UNAIR Mulyorejo, Jl Dr Ir, Surabaya, East Java 60115, Indonesia

6 Department of Pharmacy, Universitas Muhammadiyah Palangkaraya, Jl RTA Milono Km 1.5 Pahandut, Palangka Raya, Central Kalimantan 73111, Indonesia

7 Amity Inst Phytomedicine and Phytochemistry, Amity University, Amity University, Uttar Pradesh, Noida 201313, India

8 Medicinal Chemistry Research Laboratory, Birla Institute of Technology & Science Pilani (BITS Pilani), Pilani Campus, Pilani 333031, Rajasthan, India

disease [5]. To date, numerous vaccines against the novel coronavirus disease (COVID-19) were developed, giving us all hope of being free from the widespread disease. In general, vaccines are effective for prophylactic use, i.e., effective when administered prior to infection (prophylactic), but potent antiviral agents are required to treat people who already have COVID-19 infection [6, 7]. Currently, there are several repurposed drugs such as hydroxychloroquine/azithromycin, favipiravir, hydroxychloroquine, lopinavir/ritonavir, remdesivir, arbidol, and lopinavir/ritonavir combined with interferon beta [8]. In the beginning of November, two new antiviral drugs (molnupiravir and paxlovid) were reported to reduce death as well as hospitalization numbers among patients who were treated early after their initial infection in clinical studies [9]. Despite above mentioned, there is still an urgent need to look for specific antiviral drugs and additional clinical trials are needed to investigate their inhibitory mechanisms, efficacy, and safety in the treatment of coronavirus infection [10–13]. Many researchers have focused on some targets in order to discover and develop potential antivirals by blocking major steps in the life cycle of COVID-19 [14]. Targeting the lifecycle steps of SARS-CoV-2, including virus attachment, viral replication, transcription, and virus assembly and release, provides possible targets for clinical intervention [15].

The cell entry of SAR-COV-2 depends on the binding of the viral spike (S) proteins to human cellular receptors and on the S protein priming by host cell proteases [16, 17]. The viral S protein is cleaved into S1 and S2; the S1 which interacts with angiotensin-converting enzyme 2 (ACE2) and S2, which is again split and stimulated by transmembrane protease serine 2 (TMPRSS2). Therefore, the fusion of viral-host membrane will occur as a result of these actions. These high-affinity interactions are required for viral entry; they are prime targets in COVID-19 treatment. Chloroquine has previously been reported to inhibit the virus-receptor interaction in SARS-CoV infection by interfering with the terminal glycosylation of ACE2. Furthermore, both camostat and nafamostat are TMPRSS2 inhibitors that have been found to be effective against MERS-CoV in clinical trials [18–27]. Subsequently, the virus gets uncoated after entering the host body and begins genome replication, which is followed by translation at the cytoplasmic membrane, which is assisted by a coordinated RNA synthesis process mediated by a protein complex encoded by the 20 kb replicase gene [28]. In the cell, novel SARS-CoV-2-specific antiviral drugs can target the virus' main protease (M^{pro}), also known as a chymotrypsin-like cysteine protease ($3CL^{pro}$), and the papain-like protease (PL^{pro}) because of its importance in the processing of polyproteins translated from the SARS-CoV-2 RNA-dependent RNA polymerase (RdRp) or viral RNA which is needed for viral genome replication and transcription of viral genes [29–35].

In addition, drugs that target viral proteins have the potential to be more selective against the virus while causing fewer negative side effects in humans. The COVID-19 M^{pro} and PL^{pro} are intriguing as targets to safely encounter the viral disease because they are required for COVID-19 replication, are extremely conserved among related viruses, and are not found in humans [36–38]. The very recently Paxlovidis is an antiviral drug developed by Pfizer which acts as an orally active M^{pro} or 3CL protease inhibitor [39]. M^{pro} is known to be inhibited by the fixed-dose combination of ritonavir and lopinavir (Kaletra), which is allowed for the treatment of HIV/AIDS [40]. Unfortunately, the Kaletra has shown to be ineffective in treating SARS-CoV-2 in preliminary clinical trials [41]. Nevertheless, it is currently being tested in combination with other antiviral medications. Moreover, disulfiram, an alcohol-aversive medication that is available in the clinic, has been found to inhibit PL^{pro} in both SARS-CoVand MERS-CoV [42, 43]. In addition, a number of RdRp inhibitors reported being ineffective in treating COVID-19 infections were originally developed for different viruses. Remdesivir, an adenosine analog prodrug, was originally designed for the treatment of EBOV and has wide antiviral activity against RNA viruses [44]. Remdesivir therapy in animal models has been positive against infection with MERS-CoV and SARS-CoV [45, 46].

In vitro SARS-CoV-2 replication had been inhibited by remdesivir [47]. Other RdRp inhibitors include favipiravir, ribavirin, and molnupiravir [40, 48–52]. However, discovering and developing effective antiviral therapies can be costly and time-consuming. For this reason, applications of in silico ADMET/drugs-likeness prediction, molecular docking, and molecular dynamics simulations are easily explored and time-saving to search for potential perform molecules against multiple protein targets [53–57]. There are some recent studies suggesting the use of traditional herbal medicines as an adjuvant for the administration of COVID-19; therefore, efforts to integrate the use of both western medicines and drugs for designing appropriate therapy strategies are still ongoing [54–56]. Natural products are a prolific source of secondary metabolites that are molecular inspirations for drugs, which may have elevated pharmacologic properties and minimal side effects, against viral infections [57–59]. As stated, phytochemicals play a variety of roles in viruses (hepatitis C virus (HCV), herpes simplex virus (HSV), dengue, chikungunya, influenza, SARS) including genetic material and destroying nucleocapsid, inhibiting viral entrance and reducing the virus reproduction [58–71]. To date, numerous efforts describing the potential of phytochemicals from various sources as SARS-CoV-2 protein inhibitors especially against COVI-19 [60, 61].

In this manuscript, 305 phytochemicals from terpenoids, lignans, coumarins, saponins, polyphenols stilbenes, alkaloids, flavonoids, tannins, and steroids were selected based

on their reported antiviral activities to discover hit compounds for the five protein targeting various stages of the SARS-CoV-2 life cycle, i.e., virus attachments (ACE2 and TMPRSS2) and viral replication and transcription (M^{pro}, PL^{pro}, and RdRp). To discover the promising agents against SARS-CoV-2, the selected compounds were evaluated using in silico ADMET and drugs-likeness prediction, molecular docking, and molecular dynamics simulations.

Methodology

Preparation of ligand

The structure data file (SDF) format of each bioactive compounds and drugs was downloaded from NCBI PubChem database (https://pubchem.ncbi.nlm.nih.gov/). All structure data file (SDF) format of each ligand was subjected to energy minimization process utilizing the Merck molecular force field 94 (MMFF94) algorithm [72]. The PyRx software was used to save the minimized structures as PDBQT.

Preparation of receptors

The crystal structure of COVID-19 receptors, main protease (PDB ID: 6LU7), human angiotensin converting enzyme (PDB ID: 1O86), primer RNA (RdRp) (PDB ID: 7BV2), transmembrane protease serine 2 (TMPRSS2) (PDB ID: 7MEQ), and papain-like protease (PL^{pro}) (PDB ID: 6WX4) was retrieved from the RCSB website (www.rcsb.org). The water molecules, heteroatoms, and co-crystallized ligands were removed using discovery studio 2021 client [73]. The polar hydrogens and Kollman charges were added. Partial charges of the molecule were calculated using Geistenger method. The PDB files were converted into PDBQT file format using AutoDock tools [74].

Molecular docking protocol

Molecular docking simulations of the target compounds were investigated by using AutoDock Vina program [75]. The Vina software was run in exhaustiveness = 8. The binding sites was selected based on their co-crystallized ligands with the target proteins. On the basis of the native ligands in the receptors crystal structures, the coordinates of the active sites were determined (Table S1). AutoDock Vina affinity scores (kcal/mol) for all compounds were obtained and ranked using the free energy binding theory. The generated docking poses were graphically analyzed to check the interactions utilizing using discovery studio visualizer. It was also used to draft 2D and 3D figures of ligand-receptor complex.

In silico ADMET analysis

The prediction of drug-likeness and ADMET (absorption, distribution, metabolism, excretion, and toxicity) properties of the selected compounds was carried out utilizing online servers such as SwissADME, ProTox-II, and pkCSM, as reported in the literature [76].

Molecular dynamics (MD) simulation

The best complex (protein–ligand) pose of proteins1O86 and 6LU7 with ligand obtained from molecular docking was used for MD simulation. The GROMACS version 2019.2 package was utilized to investigate MD simulation analysis with GROMOS96 43a1 force field. Parameter files and topology of the withanolide were generated using the latest CGenFF through CHARMM-GUI [77, 78]. SPC water models that extended 10 Å from the protein were used to solve complex structures in a triclinic box [79]. To mimic the physiological salt concentrations, 55 Na^+ and 42 Cl^- ions (0.15 M salt) for 1O86-withanolide complex (Fig. 1a) and 33 Na^+ and 29 Cl^- ions (0.15 M salt) for 6LU7-withanolide-complex (Fig. 1b) were added to neutralize the systems. Both systems (NPT and NVT equilibration run were subjected to periodic boundary conditions at (300 K and 1.0 bar) for 100 ns simulation time using a Leap-frog MD integrator [80]. Energy minimization using the steepest descent approach with 5000 steps was used to eliminate bad contact inside the system [81]. Hydrogen bonding was examined using the gmx hbond tool. The gmx gyrate and gmx sasa tools were used to calculate the gyration radius and solvent accessible surface area, respectively. Using the gmx rmsf and gmx rms tools, the root mean square fluctuations (RMSF) and root mean square deviation (RMSD) of protein were computed. Trajectory analysis was carried out using GROMACS analysis tools [82]. Plots were generated by Grace software, and these plots were visualized via PyMol/VMD [83, 84]. Simulations were conducted using processor Intel(R) Xeon(R) CPU E5-2680 v4 @ 2.40 GHz, 64 bit.

Binding free energy calculation using MM-PBSA

The molecular mechanics approach for analyzing complex stability was used to calculate the binding free energy of the complexes. The binding free energy of protein–ligand complexes was calculated using the molecular mechanics Poisson–Boltzmann surface area (MM-PBSA). To calculate binding free energy, the last stable 30-ns trajectories assess by the RMSD plot were utilized. The frames were chosen at 200-ps intervals to cover a wide range of trajectories and to cover varied conformational space for better structure–function correlation. The entire procedure was expressed in the equation as follows:

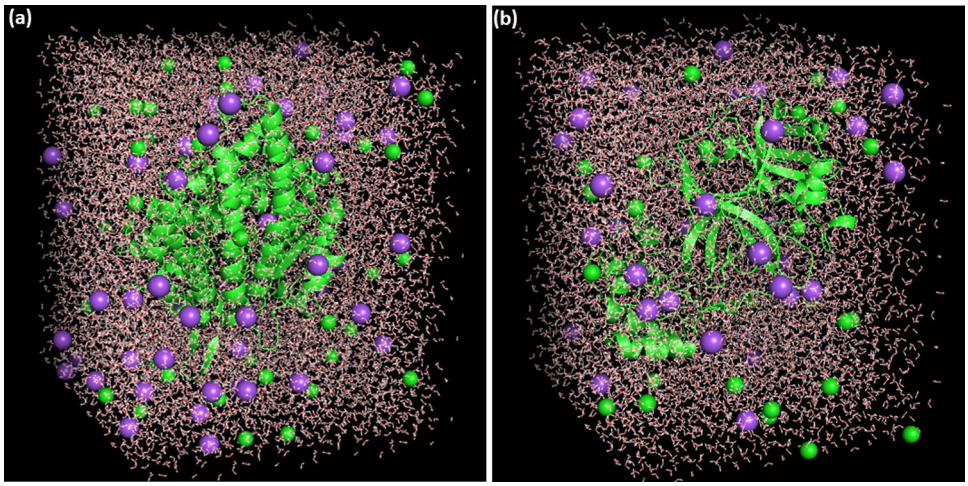

Fig. 1 Protein–ligand complex of **a** protein 1O86 and **b** protein 6LU7 in triclinic box solvated with water molecules and neutralized with 55 Na^+ and 42 Cl^- ions, and 33 Na^+ and 29 $Cl.^-$ ions (0.15 M salt), respectively

$$\Delta G_{Binding} = G_{Complex} - \left(G_{Receptor} + G_{Ligand}\right)$$

$$\Delta G_{MM-G/PBSA} = \Delta G_{vd}w + \Delta G_{ele} + \Delta G_{polar}$$

where, $G_{Complex}$ is the total MMPBSA energy of protein–ligand complex, and $G_{Receptor}$ and G_{Ligand} are the total solution free energies of the isolated receptor and ligand, respectively. Finally, the MM-G/PBSA value of the protein–ligand complex was calculated by summing the gas-phase electrostatic energy (E_{ele}), van der Waals (E_{vdW}), polar (G_{polar}), and non-polar ($G_{non\text{-}polar}$) components.

Results and discussion

Study outline

Initially, 305 alkaloids constituents, coumarins, flavonoids, lignans, phenols, saponins, steroids, stilbenes, tannins, and terpenoids obtained from PubChem were used as ligands for the current study. The absorption, distribution, metabolism, and excretion (ADME) profiles of the above-mentioned study compounds were evaluated and selected 195 ligands (Table S2) for docking study, based on Lipinski rule of five, where no violations (molecular mass less than 500 Dalton, high lipophilicity (expressed as LogP less than 5), less than 5 hydrogen bond donors and less than 10 hydrogen bond acceptors. These properties, which were followed as a strategic process in drug discovery and development, have been implemented in the current study [85]. Figure 2 shows the workflow of the overall present study.

Target receptors selection

As stated in the introduction, a full understanding the life cycle mechanism of SARS-CoV-2 is necessary in order to identify druggable targets for the discovery and development of potent coronavirus therapeutics. In the present study, we have used the potential of natural compounds derived from medicinal plants targeting the SARS-CoV-2 can be divided into two categories, with the first group targeting virus-host interactions (ACE2 (PDB ID: 1O86) and TMPRSS2 (PDB ID: 7MEQ)) or inhibiting viral enzymes (M^{pro} (PDB ID: 6LU7), PL^{pro} (PDB ID: 6WX4), and RdRp (PDB ID: 7BV2)). These targets play a major role in the viral entry, replication/transcription, and the many pharmacological target groups that can be addressed by the traditional de novo drug discovery strategy are reflected in genome and protein synthesis. Accordingly, release and assembly inhibitors are less explored steps in drug discovery against COVID-19 [86]. Despite, most of the drugs for 2019-nCoV are registered for control rather than prophylaxis; ACE2, integrin,

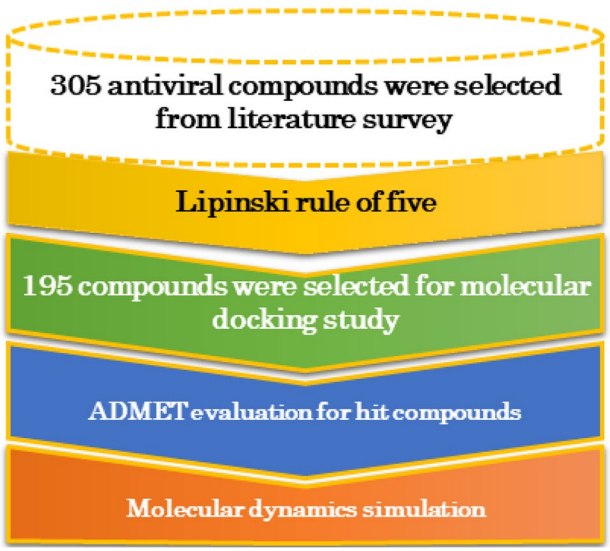

Fig. 2 Overall workflow of the present study

Table 1 Docking scores and interaction modes of top hit selected antiviral compounds with COVID-19 M.^{pro} target

No	Entry	Score Kcal/mol	Interactions	
			H-bond	Hydrophobic
9	3-HDH-withanolide F	−9.1	MET6, ILE152, ASP153, ARG298, SER301, GLY302	Alkyl: PRO9
12	Limonin	−8.7	ARG131, LYS137, LEU287	π-Alkyl: LEU286, LEU287
2	Withanolide	−8.6	LYS137, ASN238, LEU286, LEU287	Alkyl: LEU286
16	(18R)-Withaphysalin F	−8.6	ARG40, TYR54, GLU55, PHE181	
8	Obacunone	−8.6	THR199, GLY275, MET276	π-Alkyl: LEU286
89	Mimulone	−8.5	THR199, ASN238	π-Sigma: LEU272 Alkyl: VAL171, ALA194
1	Withanolide J	−8.4	TYR37, LYS88, TYR101	Alkyl: VAL35, LYS90
79	Inophyllum C	−8.4	GLN110, THR292, PRO293	π-Sigma: ILE249 π-π Stacked: PHE294 π-Alkyl: PRO293
5	Withanolide N	−8.3	MET276, ASN277, GLY278	π-Alkyl: TYR239
78	Inophyllum P	−8.3	ARG131, THR199, ASN238	

and S protein targets are important for drug repurposing or development programs aimed at preventing viral entrance and fusion. Considering the basic goal of all viruses is to transport and replicate their genetic code incompetent host cells, inhibiting the M^{pro}, PL^{pro}, ACE2, TMPRSS2, and RdRp is suggested to be promising targets for anti-2019-nCoV drug discovery of small molecules.

In addition, targeting human proteins is also a strategy to avoid viral scape caused by mutation. Another option is a multi-target strategy that combines the potential antiviral agents that acting on several targets to enhance efficacy and prevent virus resistance [87]. In light of the COVID-19 pandemic's urgency, the repurposing drugs is a better opportunity to develop a timely and effective cure. In fact, some of the pharmaceuticals currently being tested in clinical trials were originally approved for other purposes [88]. However, past and current coronavirus epidemics necessitate our preparedness not only for the immediate situation, but also for the possibility of novel coronaviruses re-emerging in the future. In this regard, finding equivalent medications that work as pancoronavirus antivirals or using a multi-target approach are crucial to minimize any loss of effectiveness due to viral mutation escape.

Molecular docking study

The total around 195 compounds were docked against five receptors including, main protease (M^{pro}) (PDB ID:

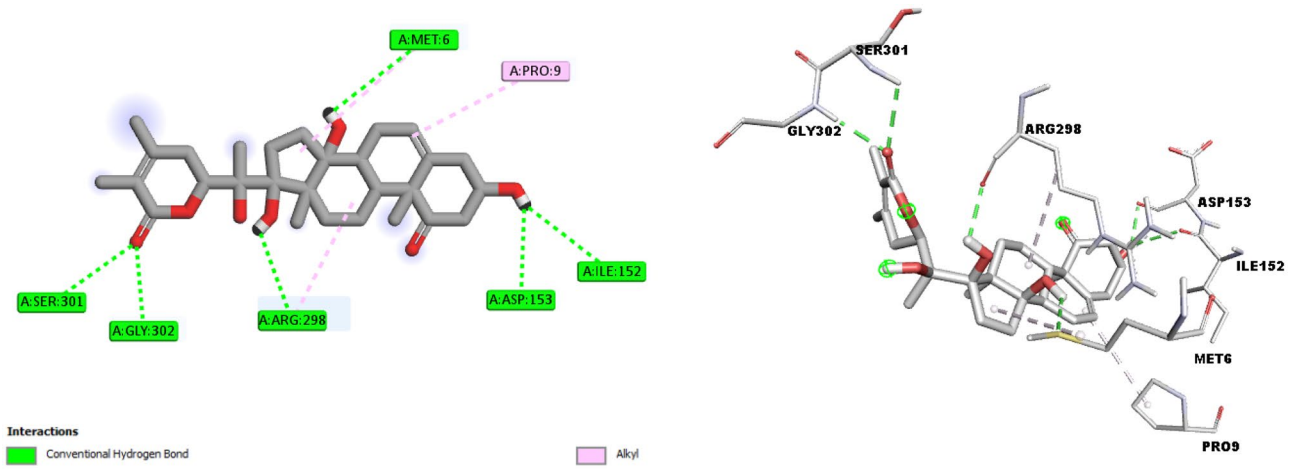

Fig. 3 Molecular interactions of 3-HDH-withanolide F with COVID-19 M.^{pro} residues (PDB ID: 6LU7)

Table 2 Docking scores and interaction modes of top hit selected antiviral compounds with COVID-19 ACE receptor

No	Entry	Score Kcal/mol	Interactions		
			H-bond	Hydrophobic	Other
2	Withanolide	−11.2	GLN281, ASN374, GLU376, HIS383, ASP415	Alkyl: PRO163, VAL380, π-Alkyl: TRP279, HIS383	
16	(18R)-Withaphysalin F	−11.2	GLN281, THR282, ALA354, HIS513	Alkyl: ALA354, VAL380, VAL518 π-Alkyl: HIS353, HIS383, HIS387, PHE512, TYR523	
13	Withasomnilide	−11.1	ASN70, ARG124, ALA356, GLU143	Alkyl: LEU139, LEU140, VAL518 π-Alkyl: HIS353, TRP357, HIS387, PHE512, HIS513	
89	Mimulone	−11.0	ALA356, GLU384, HIS387, HIS513	π-π T-shaped: TRP357 π-Alkyl: HIS353, HIS383, PHE457, HIS513, TYR523, PHE527	π-Sigma: PHE457
10	Somniferanolide	−11.0	GLY404, HIS410, GLU411, ARG522	Alkyl: MET223, PRO407, π-Alkyl: TRP357, HIS387	π-Sigma: TRP357, HIS410
12	Limonin	−10.9	HIS353, SER355, TYR394, HIS410,	π-π T-shaped: HIS353	π-Cation: HIS353
1	Withanolide J	−10.8	ARG522, GLU411	Alkyl: VAL351, VAL518 π-Alkyl: HIS353, HIS387, PHE512	π-Sigma: HIS387
9	3-HDH-withanolide F	−10.7	ASN66, GLU411	Alkyl: LEU81, LEU140, VAL518 π-Alkyl: TYR69	
14	7-Deacetylgedunin	−10.7	ALA354, ASP453, LYS454	Alkyl: VAL380 π-Alkyl: VAL379, PHE457	π-Sigma: GLU376 π-Anion: GLU376
6	Withasomniferanolide	−10.6	ASN70, SER355, ALA356, ARG522	π-Alkyl: TRP357, HIS387, HIS410	π-Sigma: TRP357, HIS387

6LU7), human angiotensin converting enzyme (PDB ID: 1O86), primer RNA (Rdrp) (PDB ID: 7BV2), transmembrane protease serine 2 (TMPRSS2) (PDB ID: 7MEQ), and papain-like protease (PL^{pro}) (PDB ID: 6WX4). Firstly, re-docking of the native ligands was performed to validate the accuracy and reliability of the docking method; the produced RMSD values were less than 2 (Table S1), which suggested that the docking protocol could be relied on for further molecular docking studies. The docking scores of all the study compounds were between −11.2 and −4.3 kcal/mol (Table S2). These compounds were compared with clinical drugs such as

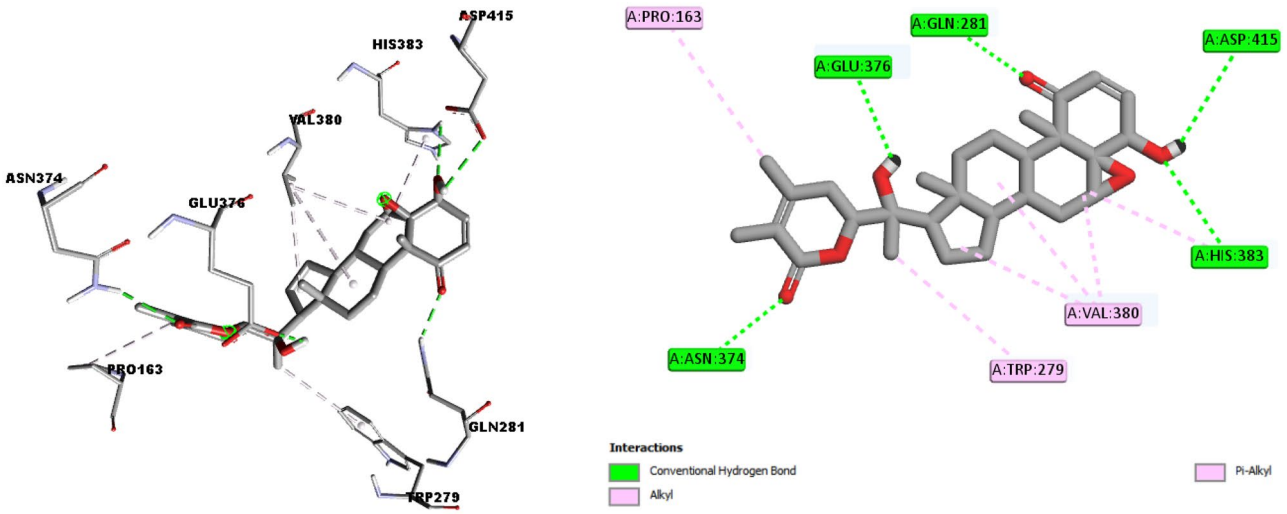

Fig. 4 Molecular interactions of withanolide with COVID-19 ACE residues (PDB ID: 1O86)

Table 3 Docking scores and interaction modes of top hit selected antiviral compounds with COVID-19 RdRp enzyme

No	Entry	Score Kcal/mol	Interactions		
			H-bond	Hydrophobic	Other
28	Aurantinidin	−8.2	ARG553, TRP617, ASP618, TYR619, ASP760		π-Anion: ASP618, ASP760
87	Tomentin A	−8.1	ASP618, ASP623, SER759, ASP760	π-Alkyl: CYS622, ALA688	π-Anion: ASP760
10	Somniferanolide	−8.0	ARG555, THR687, ASN691, ASP760		
31	Europinidin	−7.9	TYR456, ARG555, THR556, SER759	π-Alkyl: ALA688	π-Cation: ARG555 π-Anion: ASP623
91	Scutellarein	−7.8	ASN691	π-Sigma: SER682	π-Cation: ARG555 π-Anion: ASP623
29	Cyanidin	−7.8	ASP452, TYR456, ARG555, THR556		π-Anion: ASP623
31	Herbacetin	−7.7	ASN691, ASP760	π-Alkyl: ALA558 π-Sigma: SER682	π-Cation: ARG555 π-Anion: ASP623
45	Pedalitin	−7.7	ASN691, SER681, SER682	π-Sigma: SER687	π-Cation: ARG555 π-Anion: ASP623
60	Silymarin	−7.7	THR556, THR680, SER682, ASP760		π-Cation: ARG555 π-Anion: ASP623, ASP760
83	Herbacetin	−7.7	ARG555, SER682, SER759		π-Cation: ARG555 π-Anion: ASP623

ritonavir, lopinavir, hydroxychloroquine, chloroquine, favipiravir, remdesivir, camostat, nafamostat, and disulfiram (Table S3). Docking results for main protease showed that 21 compounds showed stronger binding energy in the range of −9.1 and −7.9 kcal/mol as compared to control drugs, ritonavir (−7.1 kcal/mol), and lopinavir (−7.8 kcal/mol). As shown in Table 1, main protease amino acid residues MET6, ILE152, ASP153, ARG298, SER301, and GLY302-exhibited hydrogen bond with 3-HDH-withanolide F. Additionally, the alkyl interaction with PRO9 was also observed. These interactions have resulted in the binding energy of −9.1 kcal/mol. The possible binding modes of 3-HDH-withanolide F at main protease active sites have been shown in Fig. 3.

On the other hand, ligands were docked at the active site of ACE target, and the results demonstrated that 182 ligands could inhibit target receptors with a potential energy from −11.2 to −7.0 kcal/mol, which were most potent than hydroxychloroquine (−6.8 kcal/mol) and chloroquine (−6.9 kcal/mol). It was found that withanolide exhibited the highest docking score of −11.2 kcal/mol (Table 2). As shown in Fig. 4, the molecular interactions

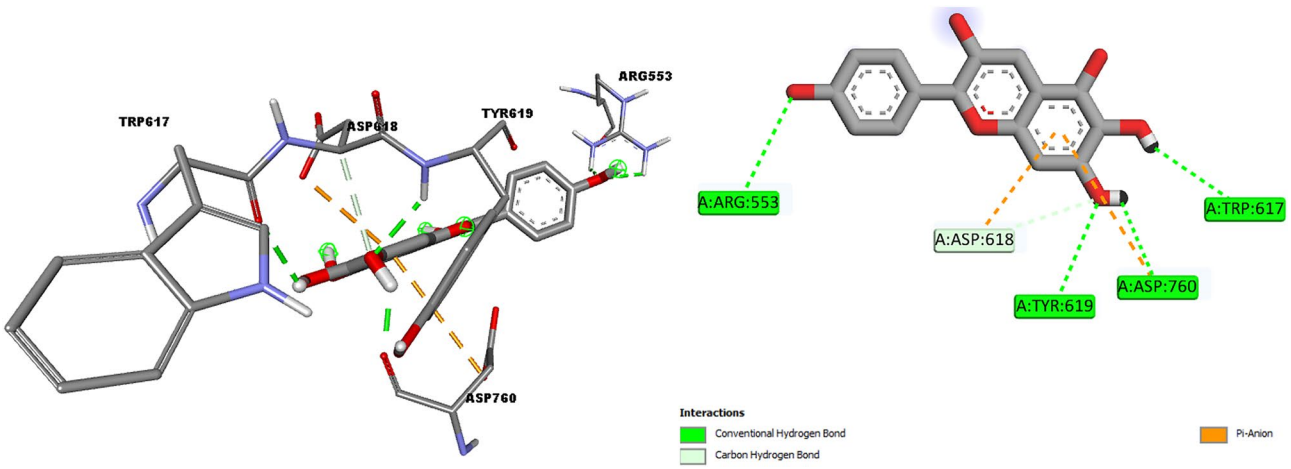

Fig. 5 Molecular interactions of aurantinidin with COVID-19 RdRp target (PDB ID: 7BV2)

Table 4 Docking scores and interaction modes of active compounds with COVID-19 TMPRSS2 receptor

No	Compound	Score Kcal/mol	Interactions		
			H-bond	Hydrophobic	Other
59	Silibinin	−8.4	VAL280, HIS296, THR393, GLY439	π-Alkyl: VAL278, VAL280, CYS281, CYS297 Alkyl: VAL280, LEU302	
60	Silymarin	−8.4	VAL280, HIS279, GLN438, GLY464	π-Sigma: VAL280 Amide-π Stacked: CYS437 π-Alkyl: CYS465	
16	(18R)-Withaphysalin F	−8.4	HIS296, SER441		
87	Tomentin A	−8.0	CYS297, SER436	π-Alkyl: CYS465	π-Cation: HIS296
89	Mimulone	−8.0	VAL280, GLN438, SER441		π-Cation: HIS296 π-Sulfur: CYS465
12	Limonin	−7.9	HIS296, GLY462, GLY464	Amide-π Stacked: TRP461	
2	Withanolide	−7.9	HIS279, THR393	Alkyl: VAL280	

holding by withanolide in the active site resulted in the formation of five H-bond with amino acid residues, namely GLN281, ASN374, GLU376, HIS383, and ASP415. Furthemore, four hydrophobic interactions were observed, including two alkyl and π-alkyl interactions with PRO163, VAL380, TRP279, and HIS383 amino acid residues.

Meanwhile, the minimum binding energies of docked ligands to the RdRp enzyme indicated that 50 of them (−7.2 to −8.2 kcal/mol) could strongly inhibit target protein as compared to the standard drugs, favipiravir, and remdesivir with binding energy of −5.8 and −7.1 kcal/mol, respectively. The ligands were ranked according to their protein–ligand binding energies, and aurantinidin was found to be the the most active compound, with binding energy of −8.2 kcal/mol (Table 3). The interactions of aurantinidin and COVID-19 RdRp established five hydrogen bonds (ARG553, TRP617, ASP618, TYR619, and ASP760) to the amino acid residues. Moreover, another interaction was also observed with ASP618 and ASP760 residues via π-anion interaction type (Fig. 5).

Transmembrane protease serine 2 (TMPRSS2) receptor has been inhibited by 7 tested compounds; the binding score of these compounds revealed that they are most active as compared to standard drugs camostat (−7.6 kcal/mol) and nafamostat (−7.7 kcal/mol) as shown in Table 4. Silibinin with a binding affinity score of −8.4 kcal/mol showed significant inhibitory activity against target receptor. The interactions between silibinin and residues in

Table 5 Docking scores and interaction modes of top hit selected antiviral compounds with COVID-19 PL^{pro} target

No	Entry	Score Kcal/mol	Interactions		
			H-bond	Hydrophobic	Other
10	Somniferanolide	−8.6	ARG166, SER170, GLN174, GLU203	π-Alkyl: TYR207 Alkyl: VAL202	
16	(18R)-Withaphysalin F	−8.3	GLU161, TYR268	π-Sigma: TYR264	
78	Inophyllum P	−8.2	TRP106, ALA288	π- π Stacked: TRP106 π-Alkyl: LYS105, ALA288	π-Cation: LYS105
1	Withanolide J	−8.2	ARG166, TYR207, LYS232	Alkyl: MET206	
79	Inophyllum C	−8.1	ALA288, LEU289	π- π Stacked: TRP106 π-Alkyl: LYS105, ALA288, LEU289	π-Cation: LYS105
89	Mimulone	−8.1	GLU161, ASP164	π-Sigma: TYR264 π-Alkyl: TYR264 Alkyl: PRO247, PRO248	π-Cation: LYS157
14	Soulattrolide	−8.1	LYS157	π- π Stacked: TYR264 π-Alkyl: PRO248	
77	Inophyllum B	−8.0	ARG166, SER170	π- π Stacked: TYR171 π-Alkyl: VAL202	
16	Absinthin	−8.0	GLU167, TYR264		
6	Withasomniferanolide	−7.9	LYS157, TYR268	Alkyl: LYS157	

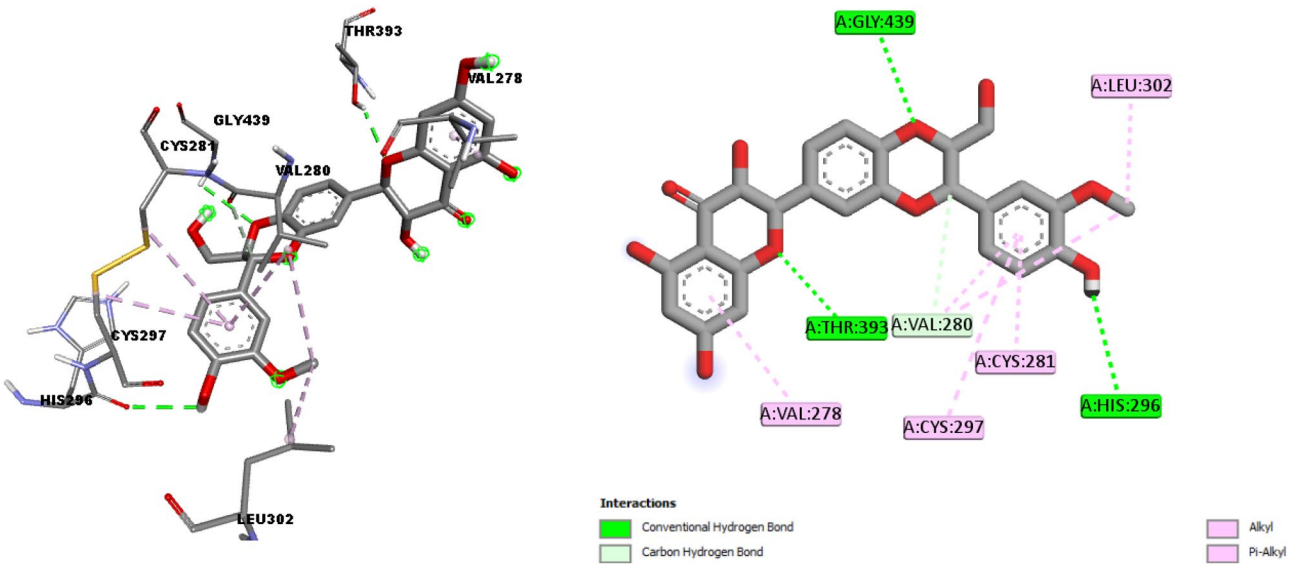

Fig. 6 Molecular interactions of silibinin with COVID-19 TMPRSS2 residues (PDB ID: 7MEQ)

TMPRSS2 were shown in Fig. 6. This compound binds with VAL280, HIS296, THR393, and GLY439 residues of receptor through H-bond. Four amino acid residues VAL278, VAL280, CYS281, and CYS297 were formed π-alkyl interaction type, whereas two alkyl interactions were also established between VAL280 and LEU302 residues and silibinin.

The results of the binding score energy of the same selected compounds for papain-like protease (PL^{pro}) protein are presented in Table S2, and 195 compounds were scored higher than disulfiram (−4.1 kcal/mol). Therefore, somniferanolide appeared as the most active inhibitor for target protein. The binding site interaction between somniferanolide and 6WX4 happens at TYR207 and VAL202 via π-alkyl and alkyl, respectively. Furthermore, four H-bonds were also observed between this compound and PL^{pro} residues including ARG166, SER170, GLN174, and GLU203 (Fig. 7) (Table 5).

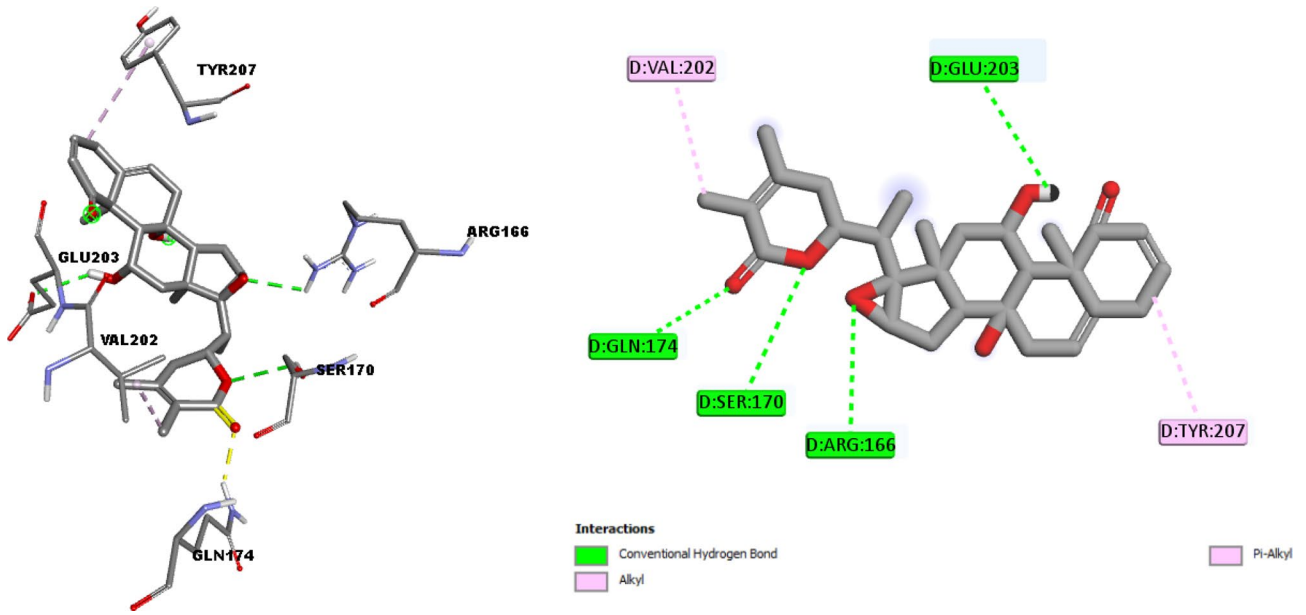

Fig. 7 Molecular interactions of somniferanolide with COVID-19 $PL.^{pro}$ residues (PDB ID: 6WX4)

Table 6 Docking scores and interaction modes of selected multitarget inhibitors of COVID-19

Target receptors	Docking scores and interactions		Multi-target inhibitors			
			Withanolide	**(18R)-Withaphysalin F**	**Limonin**	**Mimulone**
6LU7	(Kcal/mol)		−8.6	−8.6	−8.7	−8.5
	Interactions	H-bond	LYS137, ASN238, LEU286, LEU287	ARG40, TYR54, GLU55, PHE181	ARG131, LYS137, LEU287	THR199, ASN238
		Hydrophobic	Alkyl: LEU286		Alkyl: LEU286, LEU287	Alkyl: VAL171, ALA194; π-sigma: LEU272
1O86	(Kcal/mol)		−11.2	−11.2	−10.9	−11.0
	Interactions	H-bond	ASN70, ARG124, GLU143, ALA356	GLN281,THR282, ALA354, HIS513	HIS353, SER355, TYR394, HIS410, HIS513	ALA356, GLU384, HIS387, HIS513
		Hydrophobic	Alky: VAL518; π-alkyl: HIS353, PHE512, HIS513	Alky: HIS353, VAL380; π-alkyl: HIS353, HIS383	π-π T-shaped: HIS353; π-cation: HIS353	π-alkyl: HIS353, HIS383, TYR523, HIS513, PHE527; π-π T-shaped: TRP357; π-sigma: PHE457
7BV2	(Kcal/mol)		−7.5	−7.4	−7.4	−7.5
	Interactions	H-bond	ARG553, ARG555, ASN691, SER759	ARG555, THR687, ALA688	LYS545, THR687, ALA688, ASN691, SER759	ARG553, ASP761
		Hydrophobic		Alkyl: CYS622	π-alkyl: ALA688	Alkyl: LYS551, ARG555; π-cation: LYS551; π-anion: ASP618, ASP760
7MEQ	(Kcal/mol)		−7.9	−8.4	−7.9	−8.0
	Interactions	H-bond	GLN276, HIS307	HIS296, SER441	HIS296, PRO301, GLY439, SER441	VAL280, SER436, GLN438, SER441
		Hydrophobic	Alkyl: VAL280, PRO301	Alkyl: PRO301		Alkyl: VAL275, VAL278, VAL280, LEU302; π-π T-shaped: HIS296; π-cation: HIS296; π-sulfur: CYS465
6WX4	(Kcal/mol)		−7.6	−8.3	−7.7	−8.1
	Interactions	H-bond	GLN276, HIS307	GLU161, TYR268	ARG166, LYS232	GLU161, ASP164
		Hydrophobic	Alkyl: LEU185, LEU199; π-alkyl: TYR207	π-sigma: TYR264	π-alkyl: ILE222	Alkyl: PRO247, PRO248; π-alkyl: TYR264; π-cation: LYS157; π-sigma: TYR264

Table 7 In silico predicted ADMET results of selected phytochemicals

Compounds	MolWt[a]	TPSA[b]	HBD	HBA	log P	log S[c]	Caco2[d]	log BB	Rot	Acute tox.[e]	pLD_{50}[f]	Ames
Silymarin	482.441	155.14	5	10	2.3627	−3.204	0.435	−1.207	4	IV	2000	No
Limonin	470.518	104.57	0	8	3.1374	−4.379	0.952	−0.841	1	III	244	No
Withanolide	470.606	96.36	2	6	3.4954	−5.127	0.831	−0.315	2	III	300	No
Withasomnilide	470.606	96.36	2	6	3.4954	−5.209	0.834	0.022	2	II	7	No
(18R)-withaphysalin F	484.589	105.59	2	7	2.8318	−4.973	0.812	−0.422	1	II	7	No
Mimulone	408.494	86.99	3	5	5.7451	−3.817	0.651	−1.034	6	IV	2000	No
Silibinin	482.441	155.14	5	10	2.3627	−3.204	0.435	−1.207	4	IV	2000	No
Tomentin A	442.508	116.45	4	7	4.5348	−3.502	−0.366	−1.388	5	IV	2000	No
3-HDH-withanolide F	488.621	124.29	4	7	2.738	−5.209	0.668	−0.9	2	II	34	No
Somniferanolide	468.59	96.36	2	6	3.4155	−5.108	0.897	−0.347	2	II	34	No
Aurantinidin	287.247	114.29	5	6	2.9089	−2.968	−0.881	−1.612	1	V	3919	No

[a]Molecular weight in g/mol

[b]Topological polar surface area in Å.[2]

[c] Aqueous solubility in log mol/L

[d]Predicted apparent Caco-2 cell permeability in 10^{-6} cm/s

[e]Acute toxicity according to the globally harmonized system (GHS) of classification and labeling of chemicals

[f]Predicted LD_{50} in mg/kg

Worth mentioning, among docked compounds, withanolide, (18R)-withaphysalin F, limonin, and mimulone showed the highest binding affinity as compared to the selected drugs in this study. The binding scores and interaction modes of these compounds with target receptors are presented in Table 6. Therefore, the stability of withanolide complexes with each M^{pro} and ACE receptors of COVID-19 were further analyzed using MD simulations for 100-ns duration.

In silico ADMET prediction

In silico ADMET analysis of the target phytochemicals is presented in Table 7. The obtained results were compared

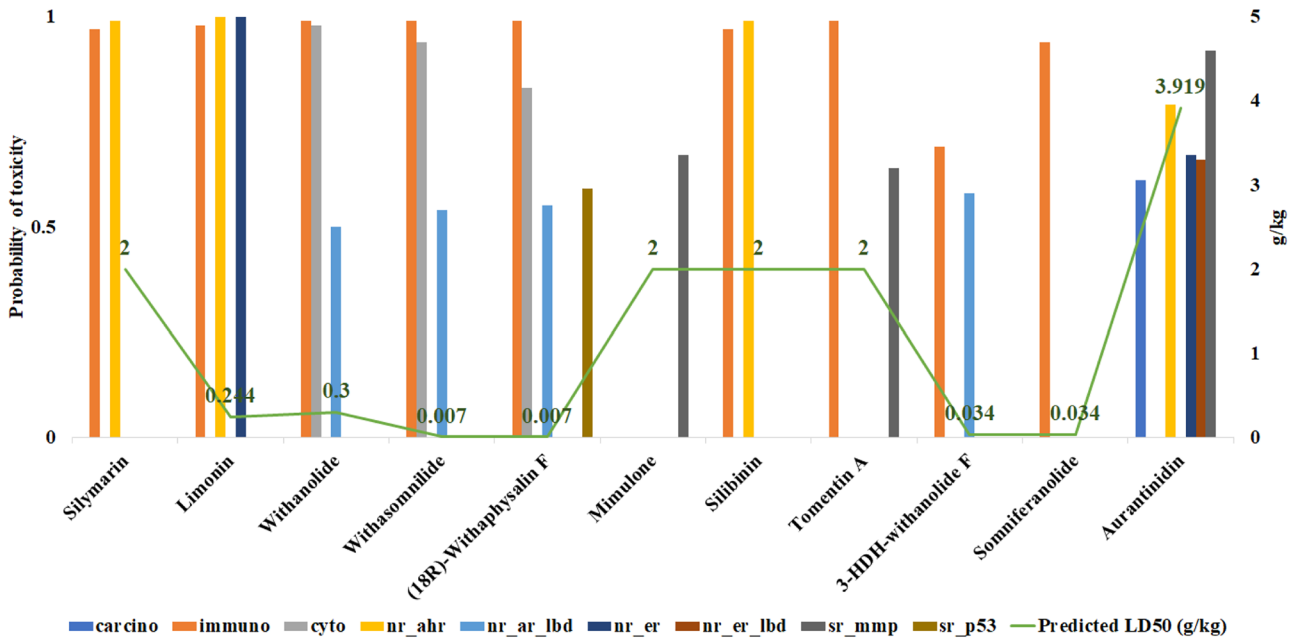

Fig. 8 In silico predicted toxicity parameters with ProTox-II

with the literature [89], as well as referring to Lipinski's rule of five (LRO5) [90]. The first parameter observed was Mol.Wt., where all compounds met the LRO5 criteria, which were ≤ 500 g/mol. Then compounds silibinin and silymarin showed TPSA values of more than 140 A^2, exceeding the criteria in LRO5 [91]. The number of hydrogen donor and acceptor groups of all compounds meets the LRO5 criteria, with no more than 5 and 10 groups,

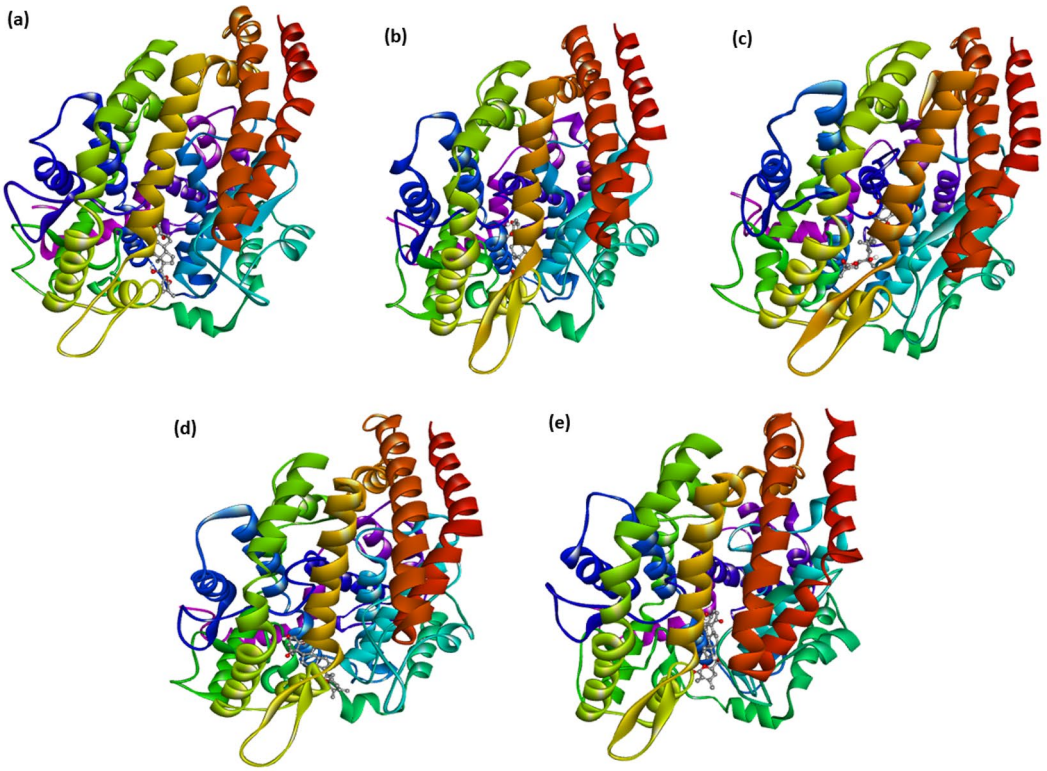

(a). 1O86-withanolide structures at **(a)** 1 ns, **(b)** 10 ns, **(c)** 20 ns, **(d)** 50 ns, and **(e)** 100 ns MD run, giving a visual impression of the sequence of events and the dynamics of the process

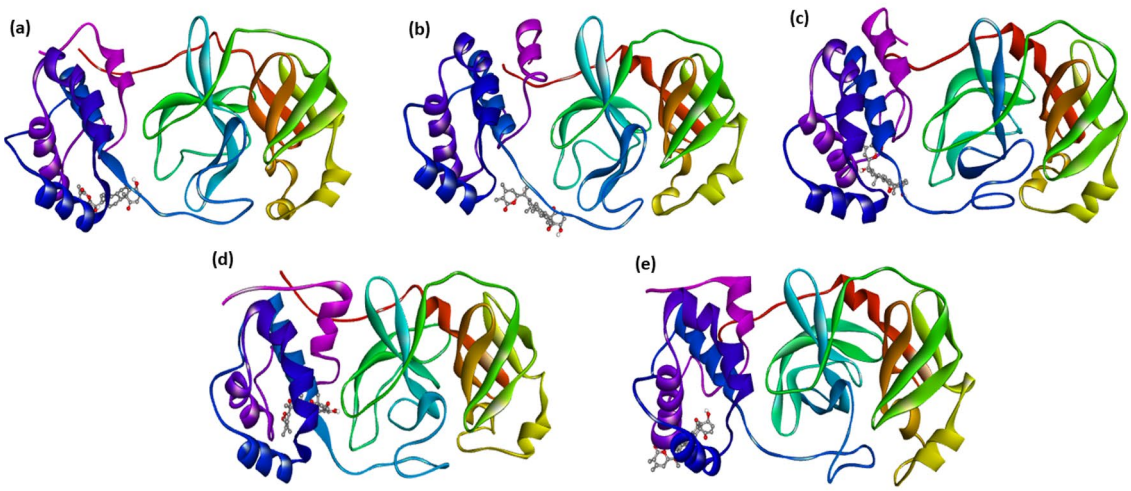

(b). 6LU7-withanolide structures at **(a)** 1 ns, **(b)** 10 ns, **(c)** 20 ns, **(d)** 50 ns, and **(e)** 100 ns MD run, giving a visual impression of the sequence of events and the dynamics of the process

Fig. 9 **a 1**O86-withanolide structures at a **1 ns,** b **10 ns,** c **20 ns,** d **50 ns, and** e 100 ns MD run, giving a visual impression of the sequence of events and the dynamics of the process. **b** 6LU7-withanolide structures at a 1 ns, b 10 ns, c 20 ns, d 50 ns, and e 100 ns MD run, giving a visual impression of the sequence of events and the dynamics of the process

respectively. One compound exceeded the LRO5 criteria for the log *P*-value: compound mimulone with log *P* of 5.75, although this value was still within the optimal range of Chander et al. [92, 93]. All compounds showed ideal log S values, although all of them were not in the optimal range of CaCo2 values. Only withasomnilide compounds were in the range of Log BB values from Chander et al. [92, 93], although they all met the criteria for the number of Rot below 15. Finally, there are four compounds (3-HDH-withanolide F, somniferanolide, withasomnilide, and (18r)-withaphysalin F) which were predicted to have high toxicity with an LD_{50} value of less than 50 mg/kg and were included in class II of the globally harmonized system of classification of labeling of chemicals (fatal if swallowed) [94], although all compounds did not showed potential as mutagens by the Ames test.

Further analysis of the target toxicity of each compound with ProTox-II is presented in Fig. 8. Some of the targets observed were potential carcinogenicity (carcino), immunotoxicity (immuno), and cytotoxicity (cyto); disrupting nuclear receptor signaling pathways on aryl hydrocarbon receptor (nr_ahr), androgen receptor ligand-binding domain (nr_ar_lbd), estrogen receptor alpha (nr_er), and estrogen receptor ligand-binding domain (nr_er_lbd), as well as interference with stress response pathways to mitochondrial membrane potential (sr_mmp) and tumor suppressor p53 (sr_p53). The results obtained were varied, with the most potential toxicity targets shown by aurantinidin with five targets in the probability range between 0.61 and 0.92. On the other hand, two compounds had the least potential toxicity targets (one target): mimulone and somniferanolide. However, the probability of somniferanolide (0.94) was much higher than mimulone (0.67). In addition, the pLD_{50} of somniferanolide (34 mg/kg) is also much lesser than mimulone (2000 mg/kg), so the potential for toxicity of mimulone was lower than somniferanolide and other compounds. Meanwhile, the most reported target of toxicity was the immunotoxicity shown by nine compounds (except mimulone and aurantinidin). Overall, ADMET results exhibited that all tested compounds possessed the drug-likeness properties. However, some compounds such as limonin, withanolide, tomentin A, and aurantinidin showed more ideal ADME properties, while the mimulone exhibited lower toxicity potential.

Molecular dynamics simulation

The molecular interactions and the solvent conditions around the protein influence the conformational stability of the protein–ligand interaction. Compounds with higher molecular interaction and docking scores have been reported to fail to bind to the protein in experimental results in various cases. Therefore, a long-range MD simulation of 100 ns was performed on docked complex in order to investigate the dynamics, conformational stability, and structural stability of protein–ligand complex. The best-docked pose with the highest binding affinity was utilized as the starting structure for the 100-ns molecular dynamics simulation run. The best

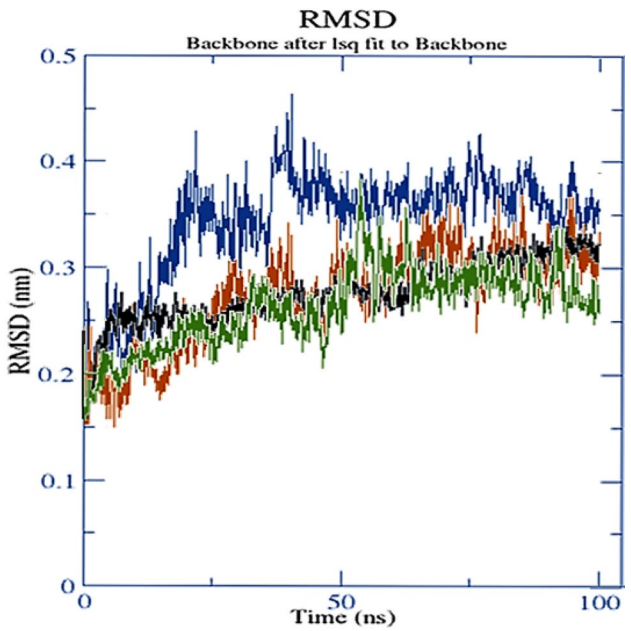

Fig. 10 The RMSD of solvated protein backbone and complex during 100 ns MD simulation (1O86-withanolide complex (green) and 6LU7-withanolide complex (brown)), and unbound 1O86 (black), unbound 6LU7 (blue)

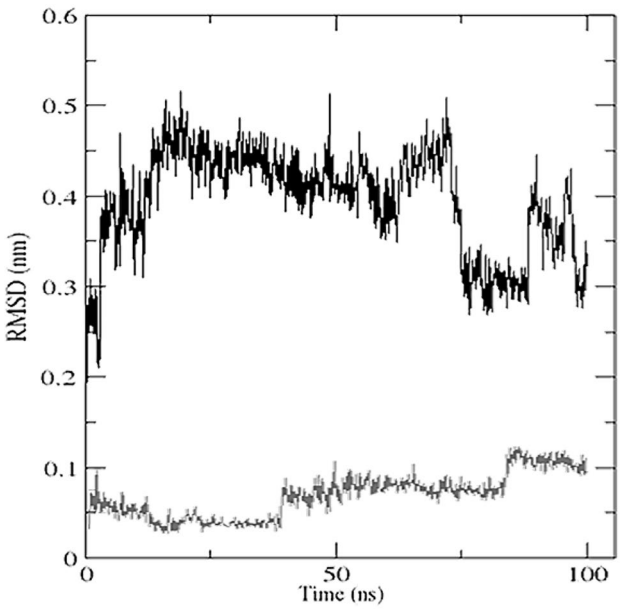

Fig. 11 RMSD of withanolide with 1O86 (black) and 6LU7 (gray) during the simulation of 100 ns

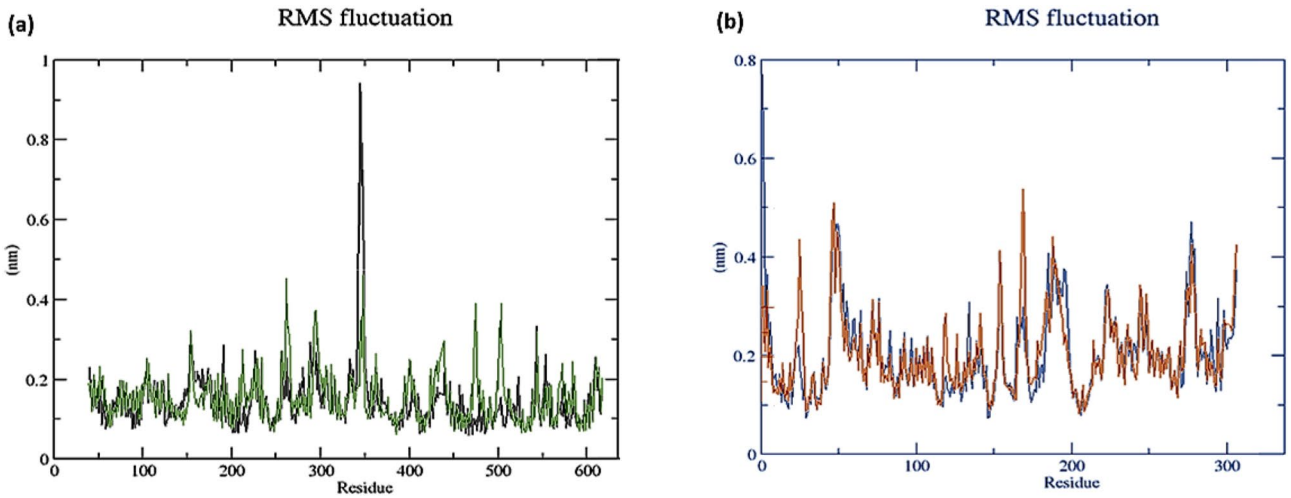

Fig. 12 The RMSF values of solvated **a** unbound 1O86 (black), 1O86-withanolide complex (green), and **b** unbound 6LU7 (blue), 6LU7-withanolide complex (brown) plotted vs amino acid numbers

pose output is employed to build up this method in a high-throughput manner for studying the binding mechanism of the complex (ligand–protein) under clearly defined water environments. The different structures represented in Fig. 9a, b give a visual impression of the sequence of events and the dynamics of the process, during 1, 10, 20, 50, and 100-ns MD simulation runs. To examine the structural stability, MD data was processed by calculating the RMSD. Complexes of 1O86 and 6LU7 with withanolide formed stable conformation after ~60 ns and ~85 ns, respectively, with an appropriate RMSD value of 2.65 and 2.91 Å, respectively, as seen in the RMSD plot (Fig. 10). The most acceptable RMSD value range is < 3.0 Å, as the lower RMSD value indicates superior stability of the system [94]. This finding shows that the withanolide develop a stable protein–ligand combination. The drop in the RMSD value of protein–ligand complexes reflects a conformational alteration in the protein secondary structure due to ligand binding. Moreover, in order to understand the conformational dynamics of withanolide in an aqueous environment, the RMSD of withanolide was also examined (Fig. 11). We observed that the conformational dynamics of withanolide in both the proteins (1O86 and 6LU7) remains stable in an aqueous solvent. However, on comparison of RMSD values, it was evident that in withanolide-1O86 complex, withanolide remains more stable than withanolide-6LU7 complex, and it was spatially occupied in the active site.

To examine the average flexibility and fluctuation of individual amino acids, the RMSF of protein and complexes was plotted from a 100-ns MD trajectory (Fig. 12). Several times during the ligand-bound state, the fluctuations of the residues in the protein could be found in the RMSF

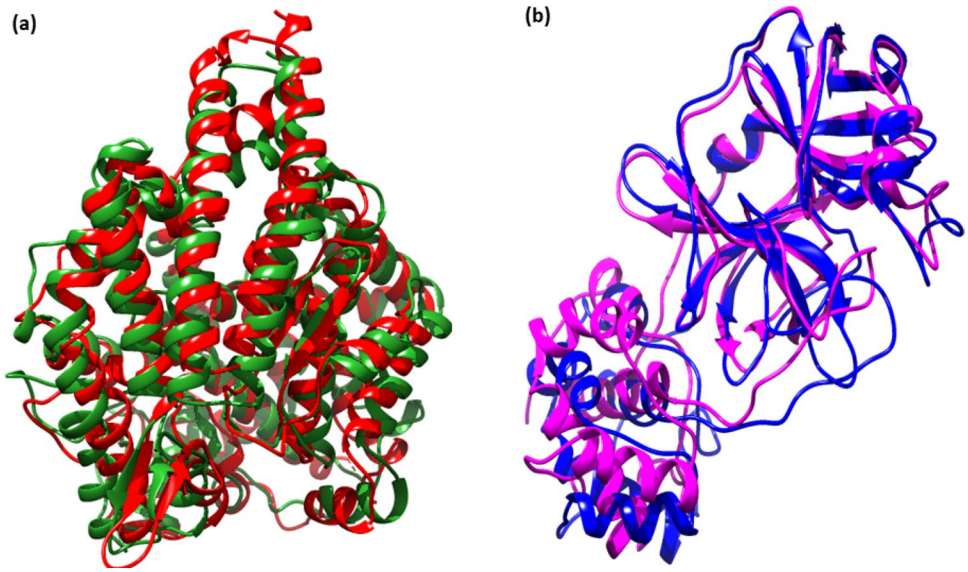

Fig. 13 Superimposed structure of **a** unbounded 1O86 (red) and 1O86 after simulation (green) and **b** unbounded 6LU7 (blue) and 6LU7 after simulation (pink)

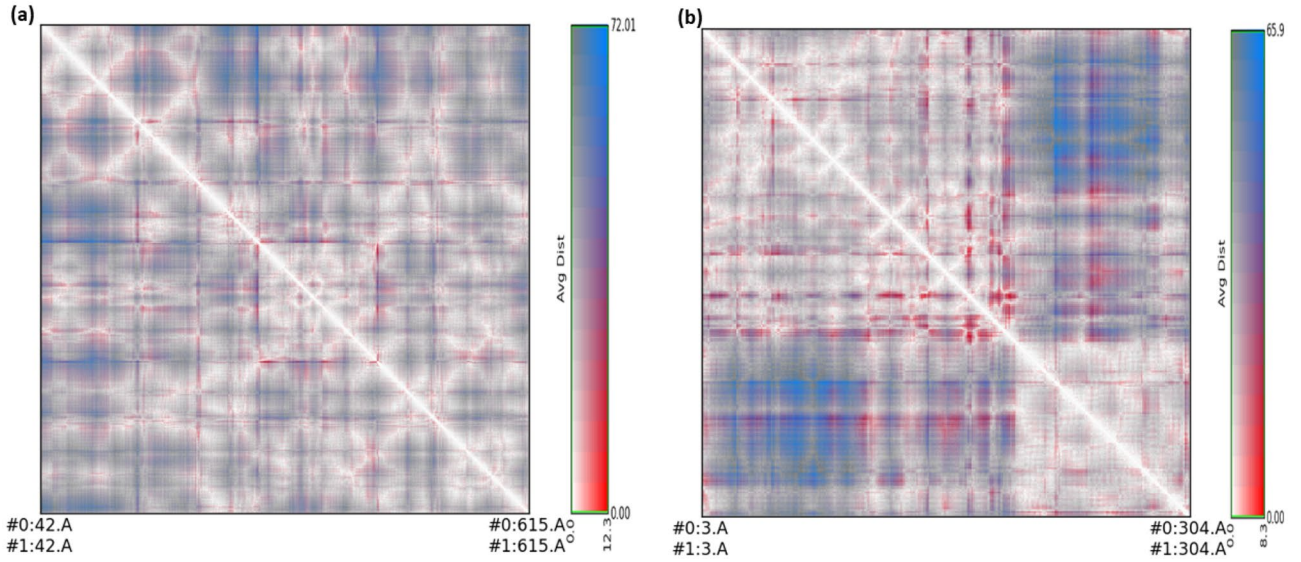

Fig. 14 RR distance map displaying patterns of spatial interactions of proteins **a** 1O86 and **b** 6LU7, showing the average distance and standard deviation for all amino acid pairs

plot. The average RMSF values of 1.481 and 1.936 Å were observed for complexes 1O86-withanolide and 6LU7-withanolide, respectively. The findings show that ligand–protein interaction brings protein chains closer and reduces the gap between them, represented in Fig. 13. The superimposed structures (Fig. 13) are obtained by Chimera 1.15 software using Tool-Structure comparison followed by MatchMaker feature. MatchMaker (or command matchmaker) performs a fit after automatically identifying which residues should be paired. Pairing uses both sequence and secondary structure, allowing similar structures to be superimposed. For evaluating and comparing protein structures, RR distance maps represent the average distance and standard deviation for all amino acid pairings between two conformations. The RR distance maps are represented in Fig. 14, which plots patterns of spatial interaction [95, 96]. The white diagonal on the map shows the 0 distance between two residues, while the red and blue elements represent residue pairings with the greatest distance variances in the two conformations. The lowest radius of gyration (Rg) value of ~23.47 and ~21.04 Å

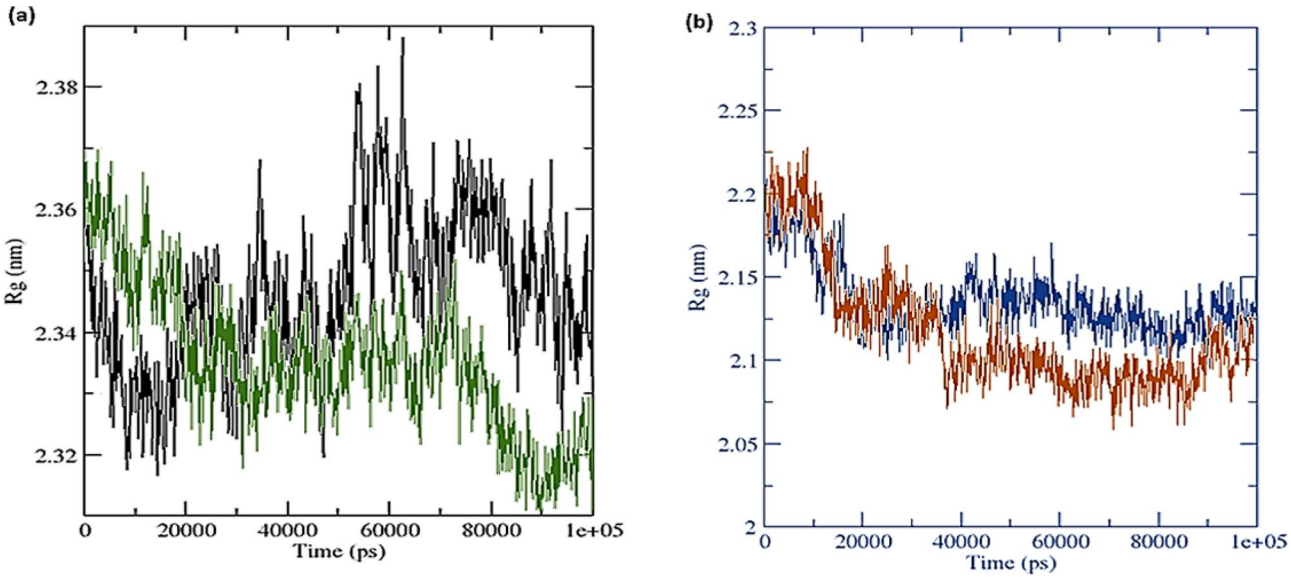

Fig. 15 Radius of gyration (Rg) **a** unbound 1O86 (black), 1O86-withanolide complex (green), and **b** unbound 6LU7 (blue) and 6LU7-withanolide complex (brown) during 100 ns simulation

was observed for 1O86-withanolide and 6LU7-withanolide complexes, respectively. Along the simulation time, Rg for the protein–ligand combination decreased, indicating that the structure became more compact (Fig. 15).

Grid-search on $17 \times 19 \times 18$ and $14 \times 18 \times 16$ grids, *rcut* = 0.35 for 1O86 and 6LU7, respectively, revealed the interactions of ligand with protein via hydrogen bonds, which were plotted against time (Fig. 16). On calculating hydrogen bonds between ligand (36 atoms) and proteins (6007 and 3038 atoms for receptors, 1O86 and 6LU7, respectively), 835 donors and 1663 acceptors were found for 1O86-withanolide complex, while 435 donors and 853 acceptors were found for the 6LU7-withanolide complex. The average number of hydrogen bonds per timeframe was observed to be 0.662 and 0.775 out of 694,302 and 185,528 possible for 1O86-withanolide and 6LU7-withanolide complexes, respectively. It can conclude that the interactions between ligand–protein substantially enhanced the number of H-bonds. Figure 17 shows the solvent accessible surface area (SASA) values changed due to binding of the ligand to the protein. The average number of SASA of 1O86-withanolide complex reduced to 222 nm^2 from 224 nm^2 for unbounded 1O86; similarly, SASA of 6LU7-withanolide complexes reduced to 132 nm^2 from 137 nm^2 for unbounded 6LU7. The reduced SASA values of protein upon ligand binding indicate that the surface of the protein exposed to the aqueous solvent was reduced due to ligand binding. It also suggests the alteration of conformation in the protein structure and reduction in pocket size with increased hydrophobicity around it [97].

Binding free energy by MM/PBSA methods

The binding free energy of the simulated complex was computed to revalidate the inhibitor affinity predicted by docking simulation studies for the 1O86-withanolide complex and 6LU7-withanolide complex. Binding free energies were calculated utilizing the final 30 ns of MD trajectories. The MM-PBSA techniques were used to compute the total nonpolar, polar, and non-bonded interaction energies (electrostatic interaction and Van der Waals) for both complexes, which are presented in Table 8.

The binding energy of 1O86-withanolide complex and 6LU7-withanolide complex was calculated to be −58.743 and −44.311 kJ/mol, respectively. The van der Waal energy of both the complexes, when compared was found that 6LU7-withanolide complex (−44.597 kJ/mol), had less binding affinity while 1O86-withanolide complex (−94.473 kJ/mol) showed strong binding affinity. In both withanolide complexes, the electrostatic energy has considerable moderate values. In both withanolide complexes, polar solvation and SASA energy showed moderate influence on binding energy. The binding energy shows the complexes stability, and 1O86-withanolide complex was found

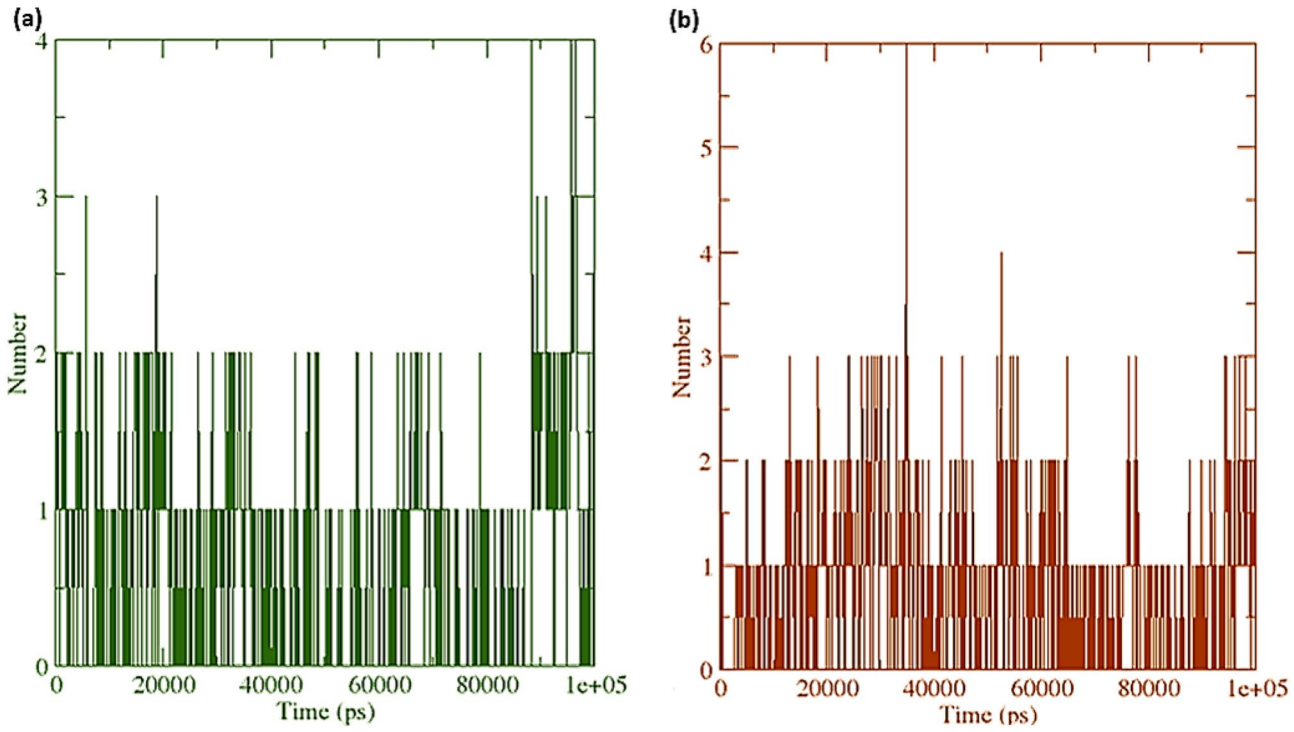

Fig. 16 Number of average hydrogen bonding interactions between **a** 1O86-withanolide complex and **b** 6LU7-withanolide complex during 100 ns simulation

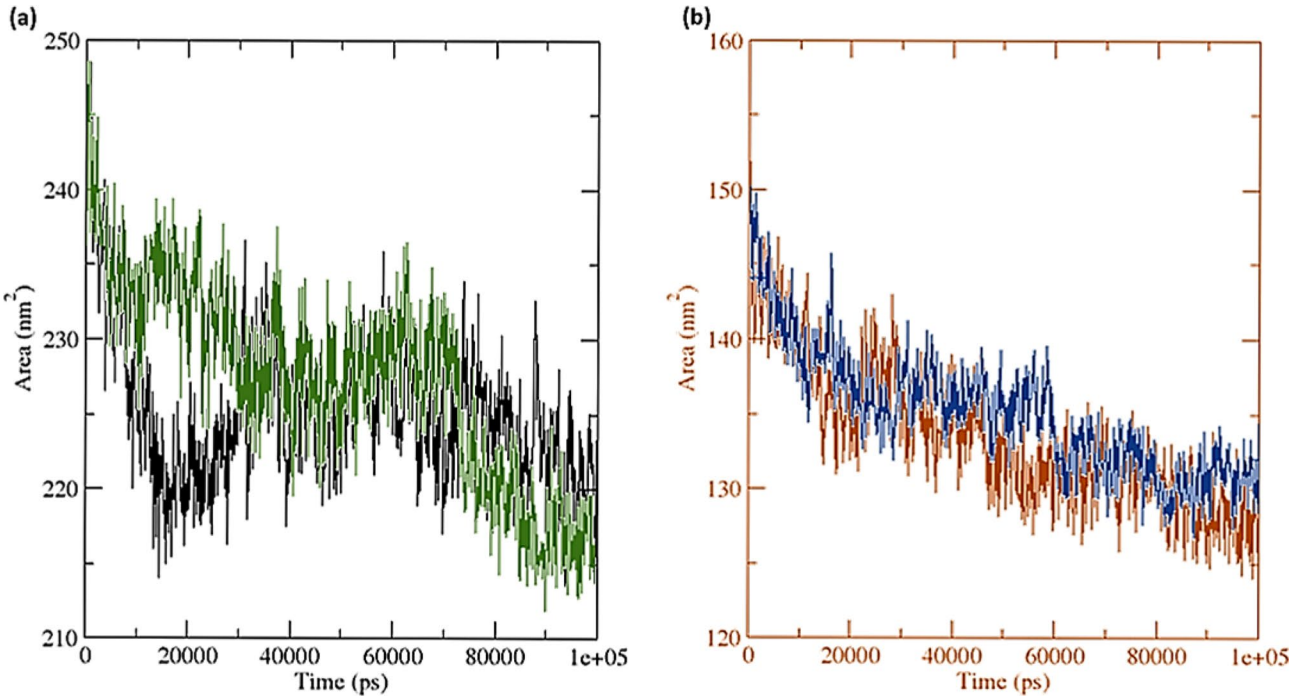

Fig. 17 Solvent accessible surface area (SASA) analysis for **a** unbound 1O86 (black), 1O86-withanolide complex (green), and **b** unbound 6LU7 (blue) and 6LU7-withanolide complex (brown) during 100 ns simulation time

Table 8 Free binding energy calculations of 1O86-withanolide and 6LU7-withanolide complexes

	1O86-withanolide complex	6LU7-withanolide complex
Binding energy (kJ/mol)	−58.743 ± 29.001	−44.311 ± 61.091
van der Waal energy (EvdW) (kJ/mol)	−94.473 ± 32.637	−44.597 ± 36.592
Electrostattic energy (Eelec) (kJ/mol)	−19.547 ± 4.694	−30.803 ± 15.171
Polar solvation energy (DG polar) (kJ/mol)	−66.448 ± 5.368	−34.146 ± 95.549
SASA energy (kJ/mol)	−25.037 ± 4.301	−19.946 ± 6.001

to be more stable comparatively and could be used as a potential inhibitor.

Conclusion

In conclusion, the current study exhibited that several phytochemicals are accomplished for the inhibition of various targets of COVID-19. Among them, withanolide, (18R)-withaphysalin F, limonin, and mimulone were active against multiple targets. Furthermore, compounds such as limonin, withanolide, tomentin A, aurantinidine, and mimulone showed more ideal ADMET properties among the compounds with the best docking results. Molecular dynamic simulation of 100 ns run revealed that both the protein–ligand complexes possess stable conformation but protein 1O86 forms a slightly more stable complex with withanolide than protein 6LU7-withanolide complex. Our findings in this study could be a good starting point for carrying out more in vitro and clinical studies to obtain potential drug candidates for the treatment of COVID-19 in the near future.

Supplementary Information The online version contains supplementary material available at https://doi.org/10.1007/s11224-022-01996-y.

Author contribution JJ, SM, and SC: supervision, investigation, and critical review; SS, HK, and MRFP: methodology, software's, investigation, formal analysis, data curation; AHH and NHAH: design of study, methodology, and writing—original draft.

Funding The authors wish to thank the Universiti Teknologi Malaysia and the Ministry of Higher Education (MOHE), Malaysia, for funding this research under the Fundamental Research Grant Scheme (FRGS/1/2019/STG01/ UTM/02/7).

Availability of data and material All data and material generated or analyzed during this study are included in the article and supplementary materials.

Code availability Not applicable.

Declarations

Conflict of interest The authors declare no competing interests.

References

1. Shahhosseini N, Babuadze G, Wong G, Kobinger GP (2021) Mutation signatures and in silico docking of novel SARS-CoV-2 variants of concern. Microorganisms 9(5):926
2. Rezaei M, Ziai SA, Fakhri S, Pouriran R (2021) ACE2: Its potential role and regulation in severe acute respiratory syndrome and COVID-19. J Cell Physiol 236(4):2430–2442. https://doi.org/10.1002/jcp.30041
3. Zaib S, Rana N, Noor A, Khan I (2021) Machine intelligence techniques for the identification and diagnosis of COVID-19. Curr Med Chem 28(26):5268–5283. https://doi.org/10.2174/0929867328666210106143307
4. World Health Organization (2021) Coronavirus (COVID-19) Dashboard. Available on: https://covid19.who.int/
5. Chen J, Lu H (2021) New challenges to fighting COVID-19: virus variants, potential vaccines, and development of antivirals. Biosci Trends 15(2):126–128. https://doi.org/10.5582/bst.2021.01092
6. Pavia CS, Wormser GP (2021) Passive immunization and its rebirth in the era of the COVID-19 pandemic. Int J Antimicrob Agents 57(3):106275. https://doi.org/10.1016/j.ijantimicag.2020.106275
7. Rehman M, Tauseef I, Aalia B, Shah SH, Junaid M, Haleem KS (2020) Therapeutic and vaccine strategies against SARS-CoV-2: past, present and future. Futur Virol. https://doi.org/10.2217/fvl-2020-0137.10.2217/fvl-2020-0137
8. Skariyachan S, Gopal D, Chakrabarti S, Kempanna P, Uttarkar A, Muddebihalkar AG, Niranjan V (2020) Structural and molecular basis of the interaction mechanism of selected drugs towards multiple targets of SARS-CoV-2 by molecular docking and dynamic simulation studies- deciphering the scope of repurposed drugs. Comput Biol Med 126:104054. https://doi.org/10.1016/j.compbiomed.2020.104054
9. Ledford H (2021) Covid antiviral pills: what scientists still want to know. Nature 599(7885):358–359. https://doi.org/10.1038/d41586-021-03074-5
10. Awadasseid A, Wu Y, Tanaka Y, Zhang W (2021) Effective drugs used to combat SARS-CoV-2 infection and the current status of vaccines. Biomed Pharmacother 137:111330. https://doi.org/10.1016/j.biopha.2021.111330
11. Poduri R, Joshi G, Jagadeesh G (2020) Drugs targeting various stages of the SARS-CoV-2 life cycle: exploring promising drugs for the treatment of Covid-19. Cell Signal 74:109721. https://doi.org/10.1016/j.cellsig.2020.109721
12. Fakhri S, Nouri Z, Moradi SZ, Akkol EK, Piri S, Sobarzo-Sánchez E, Farzaei MH, Echeverría J (2021) Targeting multiple signal transduction pathways of SARS-CoV-2: approaches to COVID-19 therapeutic candidates. Molecules 26(10):2917. https://doi.org/10.3390/molecules26102917
13. Kumar S, Sharma PP, Upadhyay C, Kempaiah P, Rathi B, Poonam (2021) Multi-targeting approach for nsp3, nsp9, nsp12 and nsp15 proteins of SARS-CoV-2 by diosmin as illustrated by molecular docking and molecular dynamics simulation methodologies. Methods 195:44–56. https://doi.org/10.1016/j.ymeth.2021.02.017
14. Elhady SS, Abdelhameed RFA, Malatani RT, Alahdal AM, Bogari HA, Almalki AJ, Mohammad KA, Ahmed SA, Khedr AIM, Darwish KM (2021) Molecular docking and dynamics simulation study of Hyrtios erectus isolated scalarane sesterterpenes as potential SARS-CoV-2 dual target inhibitors. Biology 10(5):389. https://doi.org/10.3390/biology10050389
15. Su H, Xu Y, Jiang H (2021) Drug discovery and development targeting the life cycle of SARS-CoV-2. Fundam Res 1(2):151–165. https://doi.org/10.1016/j.fmre.2021.01.013
16. Zhang H, Zhang H (2021) Entry, egress and vertical transmission of SARS-CoV-2. J Mol Cell Biol 13(3):168–174. https://doi.org/10.1093/jmcb/mjab013
17. Hu X, Shrimp JH, Guo H, Xu M, Chen CZ, Zhu W, Zakharov AV, Jain S, Shinn P, Simeonov A, Hall MD, Shen M (2021) Discovery of TMPRSS2 inhibitors from virtual screening as a potential treatment of COVID-19. ACS Pharmacol Transl Sci 4(3):1124–1135. https://doi.org/10.1021/acsptsci.0c00221
18. Hoffmann M, Kleine-Weber H, Schroeder S, Krüger N, Herrler T, Erichsen S, Schiergens TS, Herrler G, Wu N-H, Nitsche A, Müller MA, Drosten C, Pöhlmann S (2020) SARS-CoV-2 cell entry depends on ACE2 and TMPRSS2 and is blocked by a clinically proven protease inhibitor. Cell 181(2):271-280.e278. https://doi.org/10.1016/j.cell.2020.02.052
19. Vincent MJ, Bergeron E, Benjannet S, Erickson BR, Rollin PE, Ksiazek TG, Seidah NG, Nichol ST (2005) Chloroquine is a potent inhibitor of SARS coronavirus infection and spread. Virol J 2(1):69. https://doi.org/10.1186/1743-422X-2-69
20. Ren L, Xu W, Overton JL, Yu S, Chiamvimonvat N, Thai PN (2020) Assessment of chloroquine and hydroxychloroquine safety profiles: a systematic review and meta-analysis. Front Pharmacol. https://doi.org/10.3389/fphar.2020.562777
21. Yamamoto M, Matsuyama S, Li X, Takeda M, Kawaguchi Y, Inoue J-I, Matsuda Z (2016) Identification of nafamostat as a potent inhibitor of Middle East respiratory syndrome coronavirus S protein-mediated membrane fusion using the split-protein-based cell-cell fusion assay. Antimicrob Agents Chemother 60(11):6532–6539. https://doi.org/10.1128/AAC.01043-16
22. Trougakos IP, Stamatelopoulos K, Terpos E, Tsitsilonis OE, Aivalioti E, Paraskevis D, Kastritis E, Pavlakis GN, Dimopoulos MA (2021) Insights to SARS-CoV-2 life cycle, pathophysiology, and rationalized treatments that target COVID-19 clinical complications. J Biomed Sci 28(1):9. https://doi.org/10.1186/s12929-020-00703-5
23. Tang T, Bidon M, Jaimes JA, Whittaker GR, Daniel S (2020) Coronavirus membrane fusion mechanism offers a potential target for antiviral development. Antiviral Res 178:104792. https://doi.org/10.1016/j.antiviral.2020.104792
24. Faheem BK, Kumar KVGC, Sekhar S, Kunjiappan J, Jamalis R, Balaña-Fouce BLT, Sankaranarayanan M (2020) Druggable targets of SARS-CoV-2 and treatment opportunities for COVID-19. Bioorg Chem 104:104269. https://doi.org/10.1016/j.bioorg.2020.104269
25. Kishk SM, Kishk RM, Yassen ASA, Nafie MS, Nemr NA, ElMasry G, Al-Rejaie S, Simons C (2020) Molecular insights into human transmembrane protease serine-2 (TMPS2) inhibitors against SARS-CoV2: homology modelling, molecular dynamics, and docking studies. Molecules 25(21):5007. https://doi.org/10.3390/molecules25215007
26. Vardhan S, Sahoo SK (2022) Computational studies on the interaction of SARS-CoV-2 Omicron SGp RBD with human receptor ACE2, limonin and glycyrrhizic acid. Comput Biol Med 144:105367. https://doi.org/10.1016/j.compbiomed.2022.105367
27. Alazmi M, Motwalli O (2021) In silico virtual screening, characterization, docking and molecular dynamics studies of crucial SARS-CoV-2 proteins. J Biomol Struct Dyn 39(17):6761–6771. https://doi.org/10.1080/07391102.2020.1803965

28. Sola I, Almazán F, Zúñiga S, Enjuanes L (2015) Continuous and discontinuous RNA synthesis in coronaviruses. Annu Rev Virol 2(1):265–288. https://doi.org/10.1146/annurev-virology-100114-055218
29. V'kovski P, Kratzel A, Steiner S, Stalder H, Thiel V (2021) Coronavirus biology and replication: implications for SARS-CoV-2. Nat Rev Microbiol 19(3):155–170. https://doi.org/10.1038/s41579-020-00468-6
30. Wu C, Liu Y, Yang Y, Zhang P, Zhong W, Wang Y, Wang Q, Xu Y, Li M, Li X, Zheng M, Chen L, Li H (2020) Analysis of therapeutic targets for SARS-CoV-2 and discovery of potential drugs by computational methods. Acta Pharmaceutica Sinica B 10(5):766–788. https://doi.org/10.1016/j.apsb.2020.02.008
31. Marinho EM, de Andrade Neto JB, Silva J, Rocha da Silva C, Cavalcanti BC, Marinho ES, Júnior HVN (2020) Virtual screening based on molecular docking of possible inhibitors of COVID-19 main protease. Microb Pathog 148:104365. https://doi.org/10.1016/j.micpath.2020.104365
32. Huseen NHA (2020) Docking study of naringin binding with COVID-19 main protease enzyme. Iraqi J Pharm Sci (P-ISSN: 1683–3597, E-ISSN: 2521–3512) 29(2):231–238. https://doi.org/10.31351/vol29iss2pp231-238
33. Gao X, Qin B, Chen P, Zhu K, Hou P, Wojdyla JA, Wang M, Cui S (2021) Crystal structure of SARS-CoV-2 papain-like protease. Acta Pharmaceutica Sinica B 11(1):237–245. https://doi.org/10.1016/j.apsb.2020.08.014
34. Li X, Zhang L, Chen S, Ouyang H, Ren L (2021) Possible targets of pan-coronavirus antiviral strategies for emerging or re-emerging coronaviruses. Microorganisms 9(7):1479. https://doi.org/10.3390/microorganisms9071479
35. Abu-Melha S, Edrees MM, Riyadh SM, Abdelaziz MR, Elfiky AA, Gomha SM (2020) Clean grinding technique: a facile synthesis and in silico antiviral activity of hydrazones, pyrazoles, and pyrazines bearing thiazole moiety against SARS-CoV-2 main protease (Mpro). Molecules 25(19):4565
36. Kong R, Yang G, Xue R, Liu M, Wang F, Hu J, Guo X, Chang S (2020) COVID-19 Docking Server: a meta server for docking small molecules, peptides and antibodies against potential targets of COVID-19. Bioinformatics 36(20):5109–5111. https://doi.org/10.1093/bioinformatics/btaa645
37. Tang B, He F, Liu D, He F, Wu T, Fang M, Niu Z, Wu Z, Xu D (2022) AI-Aided Design of Novel Targeted Covalent Inhibitors against SARS-CoV-2. Biomolecules 12(6):746. https://doi.org/10.3390/biom12060746
38. Banerjee R, Perera L, Tillekeratne LMV (2021) Potential SARS-CoV-2 main protease inhibitors. Drug Discov Today 26(3):804–816. https://doi.org/10.1016/j.drudis.2020.12.005
39. Vandyck K, Deval J (2021) Considerations for the discovery and development of 3-chymotrypsin-like cysteine protease inhibitors targeting SARS-CoV-2 infection. Curr Opin Virol 49:36–40. https://doi.org/10.1016/j.coviro.2021.04.006
40. Dong L, Hu S, Gao J (2020) Discovering drugs to treat coronavirus disease 2019 (COVID-19). Drug Discov Ther 14(1):58–60. https://doi.org/10.5582/ddt.2020.01012
41. Cao B, Wang Y, Wen D, Liu W, Wang J, Fan G, Ruan L, Song B, Cai Y, Wei M, Li X, Xia J, Chen N, Xiang J, Yu T, Bai T, Xie X, Zhang L, Li C, Yuan Y, Chen H, Li H, Huang H, Tu S, Gong F, Liu Y, Wei Y, Dong C, Zhou F, Gu X, Xu J, Liu Z, Zhang Y, Li H, Shang L, Wang K, Li K, Zhou X, Dong X, Qu Z, Lu S, Hu X, Ruan S, Luo S, Wu J, Peng L, Cheng F, Pan L, Zou J, Jia C, Wang J, Liu X, Wang S, Wu X, Ge Q, He J, Zhan H, Qiu F, Guo L, Huang C, Jaki T, Hayden FG, Horby PW, Zhang D, Wang C (2020) A Trial of lopinavir-ritonavir in adults hospitalized with severe COVID-19. N Engl J Med 382(19):1787–1799. https://doi.org/10.1056/NEJMoa2001282
42. Anirudhan V, Lee H, Cheng H, Cooper L, Rong L (2021) Targeting SARS-CoV-2 viral proteases as a therapeutic strategy to treat COVID-19. J Med Virol 93(5):2722–2734. https://doi.org/10.1002/jmv.26814
43. Lin M-H, Moses DC, Hsieh C-H, Cheng S-C, Chen Y-H, Sun C-Y, Chou C-Y (2018) Disulfiram can inhibit MERS and SARS coronavirus papain-like proteases via different modes. Antiviral Res 150:155–163. https://doi.org/10.1016/j.antiviral.2017.12.015
44. Yin W, Mao C, Luan X, Shen D-D, Shen Q, Su H, Wang X, Zhou F, Zhao W, Gao M, Chang S, Xie Y-C, Tian G, Jiang H-W, Tao S-C, Shen J, Jiang Y, Jiang H, Xu Y, Zhang S, Zhang Y, Xu HE (2020) Structural basis for inhibition of the RNA-dependent RNA polymerase from SARS-CoV-2 by remdesivir. Science 368(6498):1499–1504. https://doi.org/10.1126/science.abc1560
45. de Wit E, Feldmann F, Cronin J, Jordan R, Okumura A, Thomas T, Scott D, Cihlar T, Feldmann H (2020) Prophylactic and therapeutic remdesivir (GS-5734) treatment in the rhesus macaque model of MERS-CoV infection. Proc Natl Acad Sci 117(12):6771–6776. https://doi.org/10.1073/pnas.1922083117
46. Sheahan TP, Sims AC, Leist SR, Schäfer A, Won J, Brown AJ, Montgomery SA, Hogg A, Babusis D, Clarke MO, Spahn JE, Bauer L, Sellers S, Porter D, Feng JY, Cihlar T, Jordan R, Denison MR, Baric RS (2020) Comparative therapeutic efficacy of remdesivir and combination lopinavir, ritonavir, and interferon beta against MERS-CoV. Nat Commun 11(1):222. https://doi.org/10.1038/s41467-019-13940-6
47. Wang M, Cao R, Zhang L, Yang X, Liu J, Xu M, Shi Z, Hu Z, Zhong W, Xiao G (2020) Remdesivir and chloroquine effectively inhibit the recently emerged novel coronavirus (2019-nCoV) in vitro. Cell Res 30(3):269–271. https://doi.org/10.1038/s41422-020-0282-0
48. Singh TU, Parida S, Lingaraju MC, Kesavan M, Kumar D, Singh RK (2020) Drug repurposing approach to fight COVID-19. Pharmacol Rep 72(6):1479–1508. https://doi.org/10.1007/s43440-020-00155-6
49. Malone B, Campbell EA (2021) Molnupiravir: Coding for catastrophe. Nat Struct Mol Biol 28(9):706–708. https://doi.org/10.1038/s41594-021-00657-8
50. Naveed M, Tehreem S, Arshad S, Bukhari SA, Shabbir MA, Essa R, Ali N, Zaib S, Khan A, Al-Harrasi A, Khan I (2021) Design of a novel multiple epitope-based vaccine: an immunoinformatics approach to combat SARS-CoV-2 strains. J Infect Public Health 14(7):938–946. https://doi.org/10.1016/j.jiph.2021.04.010
51. Zhang S, Pei R, Li M, Su H, Sun H, Ding Y, Su M, Huang C, Chen X, Du Z, Jin C, Zang Y, Li J, Xu Y, Chen X, Zhang B, Ding K (2022) Cocktail polysaccharides isolated from Ecklonia kurome against the SARS-CoV-2 infection. Carbohyd Polym 275:118779. https://doi.org/10.1016/j.carbpol.2021.118779
52. Naydenova K, Muir KW, Wu L-F, Zhang Z, Coscia F, Peet MJ, Castro-Hartmann P, Qian P, Sader K, Dent K, Kimanius D, Sutherland JD, Löwe J, Barford D, Russo CJ (2021) Structure of the SARS-CoV-2 RNA-dependent RNA polymerase in the presence of favipiravir-RTP. Proc Natl Acad Sci 118(7):e2021946118. https://doi.org/10.1016/j.ultramic.2021.113396
53. Vardhan S, Sahoo SK (2020) In silico ADMET and molecular docking study on searching potential inhibitors from limonoids and triterpenoids for COVID-19. Comput Biol Med 124:103936. https://doi.org/10.1016/j.compbiomed.2020.103936
54. Vijesh AM, Isloor AM, Telkar S, Arulmoli T, Fun H-K (2013) Molecular docking studies of some new imidazole derivatives for antimicrobial properties. Arab J Chem 6(2):197–204. https://doi.org/10.1016/j.arabjc.2011.10.007
55. Alfarisi S, Santoso M, Kristanti AN, Siswanto I, Puspaningsih NNT (2020) synthesis, antimicrobial study, and molecular docking simulation of 3,4-dimethoxy-β-nitrostyrene derivatives as

candidate PTP1B inhibitor. Sci Pharm 88(3):37. https://doi.org/10.3390/scipharm88030037
56. Abu-Melha S, Edrees MM, Said MA, Riyadh SM, Al-Kaff NS, Gomha SM (2022) Potential COVID-19 drug candidates based on diazinyl-thiazol-imine moieties: synthesis and greener pastures biological study. Molecules 27(2):488. https://doi.org/10.3390/molecules27020488
57. Jain R, Mujwar S (2020) Repurposing metocurine as main protease inhibitor to develop novel antiviral therapy for COVID-19. Struct Chem 31(6):2487–2499. https://doi.org/10.1007/s11224-020-01605-w
58. Anand AV, Balamuralikrishnan B, Kaviya M, Bharathi K, Parithathvi A, Arun M, Senthilkumar N, Velayuthaprabhu S, Saradhadevi M, Al-Dhabi NA, Arasu MV, Yatoo MI, Tiwari R, Dhama K (2021) Medicinal plants, phytochemicals, and herbs to combat viral pathogens including SARS-CoV-2. Molecules 26(6):1775. https://doi.org/10.3390/molecules26061775
59. Fakhri S, Piri S, Majnooni MB, Farzaei MH, Echeverría J (2020) Targeting neurological manifestations of coronaviruses by candidate phytochemicals: a mechanistic approach. Front Pharmacol 11:621099. https://doi.org/10.3389/fphar.2020.621099
60. Parida PK, Paul D, Chakravorty D (2021) Nature's therapy for COVID-19: Targeting the vital non-structural proteins (NSP) from SARS-CoV-2 with phytochemicals from Indian medicinal plants. Phytomedicine Plus 1(1):100002. https://doi.org/10.1016/j.phyplu.2020.100002
61. Lalani S, Poh CL (2020) Flavonoids as Antiviral Agents for Enterovirus A71 (EV-A71). Viruses. https://doi.org/10.3390/v12020184
62. Khan SL, Siddiqui FA, Jain SP, Sonwane GM (2021) Discovery of potential inhibitors of SARS-CoV-2 (COVID-19) main protease (M^{pro}) from *Nigella Sativa* (Black Seed) by molecular docking study. Coronaviruses 2(3):384–402. https://doi.org/10.2174/2666796701999200921094103
63. Ben-Shabat S, Yarmolinsky L, Porat D, Dahan A (2020) Antiviral effect of phytochemicals from medicinal plants: applications and drug delivery strategies. Drug Deliv Transl Res 10(2):354–367. https://doi.org/10.1007/s13346-019-00691-6
64. Kim C-H (2021) Anti–SARS-CoV-2 Natural products as potentially therapeutic agents. Front Pharmacol 12:1015. https://doi.org/10.3389/fphar.2021.590509
65. Fielding BC, Filho CDSMB, Ismail NSM, Sousa DP (2020) Alkaloids: therapeutic potential against human coronaviruses. Molecules. https://doi.org/10.3390/molecules25235496
66. Diniz LRL, Perez-Castillo Y, Elshabrawy HA, Filho CDSMB, de Sousa DP (2021) Bioactive terpenes and their derivatives as potential SARS-CoV-2 proteases inhibitors from molecular modeling studies. Biomolecules 11(1):74. https://doi.org/10.3390/biom11010074
67. Abdelmohsen UR, Albohy A, Abdulrazik BS, Bayoumi SAL, Malak LG, Khallaf ISA, Bringmann G, Farag SF (2021) Natural coumarins as potential anti-SARS-CoV-2 agents supported by docking analysis. RSC Adv 11(28):16970–16979. https://doi.org/10.1039/D1RA01989A
68. Wahedi HM, Ahmad S, Abbasi SW (2021) Stilbene-based natural compounds as promising drug candidates against COVID-19. J Biomol Struct Dyn 39(9):3225–3234. https://doi.org/10.1080/07391102.2020.1762743
69. Xu X-Y, Wang D-Y, Li Y-P, Deyrup ST, Zhang H-J (2021) Plant-derived lignans as potential antiviral agents: a systematic review. Phytochem Rev. https://doi.org/10.1007/s11101-021-09758-0
70. Pandey P, Rane JS, Chatterjee A, Kumar A, Khan R, Prakash A, Ray S (2021) Targeting SARS-CoV-2 spike protein of COVID-19 with naturally occurring phytochemicals: an in silico study for drug development. J Biomol Struct Dyn 39(16):6306–6316. https://doi.org/10.1080/07391102.2020.1796811
71. Daoui O, Mazoir N, Bakhouch M, Salah M, Benharref A, Gonzalez-Coloma A, Elkhattabi S, Yazidi ME, Chtita S (2022) 3D-QSAR, ADME-Tox, and molecular docking of semisynthetic triterpene derivatives as antibacterial and insecticide agents. Struct Chem. https://doi.org/10.1007/s11224-022-01912-4
72. Akdemir A, Angeli A, Göktaş F, Eraslan Elma P, Karalı N, Supuran CT (2019) Novel 2-indolinones containing a sulfonamide moiety as selective inhibitors of candida β-carbonic anhydrase enzyme. J Enzyme Inhib Med Chem 34(1):528–531
73. Dassault Systèmes BIOVIA Discovery studio modeling environment, release 2017. Dassaul Systèmes, San Diego
74. Morris GM, Goodsell DS, Halliday RS, Huey R, Hart WE, Belew RK, Olson AJ (1998) Automated docking using a Lamarckian genetic algorithm and an empirical binding free energy function. J Comput Chem 19(14):1639–1662. https://doi.org/10.1002/(SICI)1096-987X(19981115)19:14%3c1639::AID-JCC10%3e3.0.CO;2-B
75. Trott O, Olson AJ (2010) AutoDock Vina: improving the speed and accuracy of docking with a new scoring function, efficient optimization, and multithreading. J Comput Chem 31(2):455–461. https://doi.org/10.1002/jcc.21334
76. Pratama MRF, Poerwono H, Siswodiharjo S (2019) ADMET properties of novel 5-O-benzoylpinostrobin derivatives. J Basic Clin Physiol Pharmacol. https://doi.org/10.1515/jbcpp-2019-0251
77. Vanommeslaeghe K, Hatcher E, Acharya C, Kundu S, Zhong S, Shim J, Darian E, Guvench O, Lopes P, Vorobyov I, Mackerell AD Jr (2010) CHARMM general force field: a force field for drug-like molecules compatible with the CHARMM all-atom additive biological force fields. J Comput Chem 31(4):671–690. https://doi.org/10.1002/jcc.21367
78. Yu W, He X, Vanommeslaeghe K, MacKerell AD Jr (2012) Extension of the CHARMM general force field to sulfonyl-containing compounds and its utility in biomolecular simulations. J Comput Chem 33(31):2451–2468. https://doi.org/10.1002/jcc.23067
79. Jorgensen WL, Chandrasekhar J, Madura JD, Impey RW, Klein ML (1983) Comparison of simple potential functions for simulating liquid water. J Chem Phys 79(2):926–935. https://doi.org/10.1063/1.445869
80. Allen MP, Tildesley DJ (2017) Computer simulation of liquids. Oxford university press
81. Essmann U, Perera L, Berkowitz ML, Darden T, Lee H, Pedersen LG (1995) A smooth particle mesh Ewald method. J Chem Phys 103(19):8577–8593. https://doi.org/10.1063/1.470117
82. Steinbach PJ, Brooks BR (1994) New spherical-cutoff methods for long-range forces in macromolecular simulation. J Comput Chem 15(7):667–683. https://doi.org/10.1002/jcc.540150702
83. Humphrey W, Dalke A, Schulten K (1996) VMD: visual molecular dynamics. J Mol Graph 14(1):33–38. https://doi.org/10.1016/0263-7855(96)00018-5
84. DeLano WL (2002) Pymol: An open-source molecular graphics tool. CCP4 Newsl Protein Crystallogr. 40(1):82–92
85. Su X, Kong L, Lei X, Hu L, Ye M, Zou H (2007) Biological fingerprinting analysis of traditional Chinese medicines with targeting ADME/Tox property for screening of bioactive compounds by chromatographic and MS methods. Mini Rev Med Chem 7(1):87–98. https://doi.org/10.2174/138955707779317830
86. Gil C, Ginex T, Maestro I, Nozal V, Barrado-Gil L, Cuesta-Geijo MÁ, Urquiza J, Ramírez D, Alonso C, Campillo NE, Martinez A (2020) COVID-19: drug targets and potential treatments. J Med Chem 63(21):12359–12386. https://doi.org/10.1021/acs.jmedchem.0c00606
87. Das G, Ghosh S, Garg S, Ghosh S, Jana A, Samat R, Mukherjee N, Roy R, Ghosh S (2020) An overview of key potential therapeutic strategies for combat in the COVID-19 battle. RSC Adv 10(47):28243–28266. https://doi.org/10.1039/D0RA05434H
88. Liu C, Zhou Q, Li Y, Garner LV, Watkins SP, Carter LJ, Smoot J, Gregg AC, Daniels AD, Jervey S, Albaiu D (2020) Research and development on therapeutic agents and vaccines for COVID-19

and related human coronavirus diseases. ACS Cent Sci 6(3):315–331. https://doi.org/10.1021/acscentsci.0c00272
89. Hasan AH, Murugesan S, Amran SI, Chander S, Alanazi MM, Hadda TB, Shakya S, Pratama MRF, Das B, Biswas S, Jamalis J (2022) Novel thiophene Chalcones-Coumarin as acetylcholinesterase inhibitors: design, synthesis, biological evaluation, molecular docking, ADMET prediction and molecular dynamics simulation. Bioorg Chem 119:105572. https://doi.org/10.1016/j.bioorg.2021.105572
90. Prasanna S, Doerksen JR (2009) Topological polar surface area: a useful descriptor in 2D-QSAR. Curr Med Chem 16(1):21–41. https://doi.org/10.2174/092986709787002817
91. Banerjee P, Eckert AO, Schrey AK, Preissner R (2018) ProTox-II: a webserver for the prediction of toxicity of chemicals. Nucleic Acids Res 46(W1):W257–W263. https://doi.org/10.1093/nar/gky318
92. Chander S, Ashok P, Zheng Y-T, Wang P, Raja KS, Taneja A, Murugesan S (2016) Design, synthesis and in-vitro evaluation of novel tetrahydroquinoline carbamates as HIV-1 RT inhibitor and their antifungal activity. Bioorg Chem 64:66–73. https://doi.org/10.1016/j.bioorg.2015.12.005
93. Chander S, Wang P, Ashok P, Yang L-M, Zheng Y-T, Murugesan S (2016) Rational design, synthesis, anti-HIV-1 RT and antimicrobial activity of novel 3-(6-methoxy-3,4-dihydroquinolin-1(2H)-yl)-1-(piperazin-1-yl)propan-1-one derivatives. Bioorg Chem 67:75–83. https://doi.org/10.1016/j.bioorg.2016.05.009
94. Kufareva I, Abagyan R (2012) Methods of protein structure comparison. Methods Mol Biol 857:231–257. https://doi.org/10.1007/978-1-61779-588-6_10
95. Wu S, Zhang Y (2008) A comprehensive assessment of sequence-based and template-based methods for protein contact prediction. Bioinformatics 24(7):924–931. https://doi.org/10.1093/bioinformatics/btn069
96. Khan MD, Shakya S, Thi Vu HH, Habte L, Ahn JW (2021) Low concentrated phosphorus sorption in aqueous medium on aragonite synthesized by carbonation of seashells: optimization, kinetics, and mechanism study. J Environ Manag. 280:111652. https://doi.org/10.1016/j.jenvman.2020.111652
97. Alhomrani M, Alsanie WF, Alamri AS, Alyami H, Habeeballah H, Alkhatabi HA, Felimban RI, Haynes JM, Shakya S, Raafat BM, Refat MS, Gaber A (2022) Enhancing the antipsychotic effect of risperidone by increasing its binding affinity to serotonin receptor via picric acid: a molecular dynamics simulation. Pharmaceuticals 15(3):285. https://doi.org/10.3390/ph15030285